iScience

CellPress
OPEN ACCESS

Article

Enhanced and sustained T cell activation in response to fluid shear stress

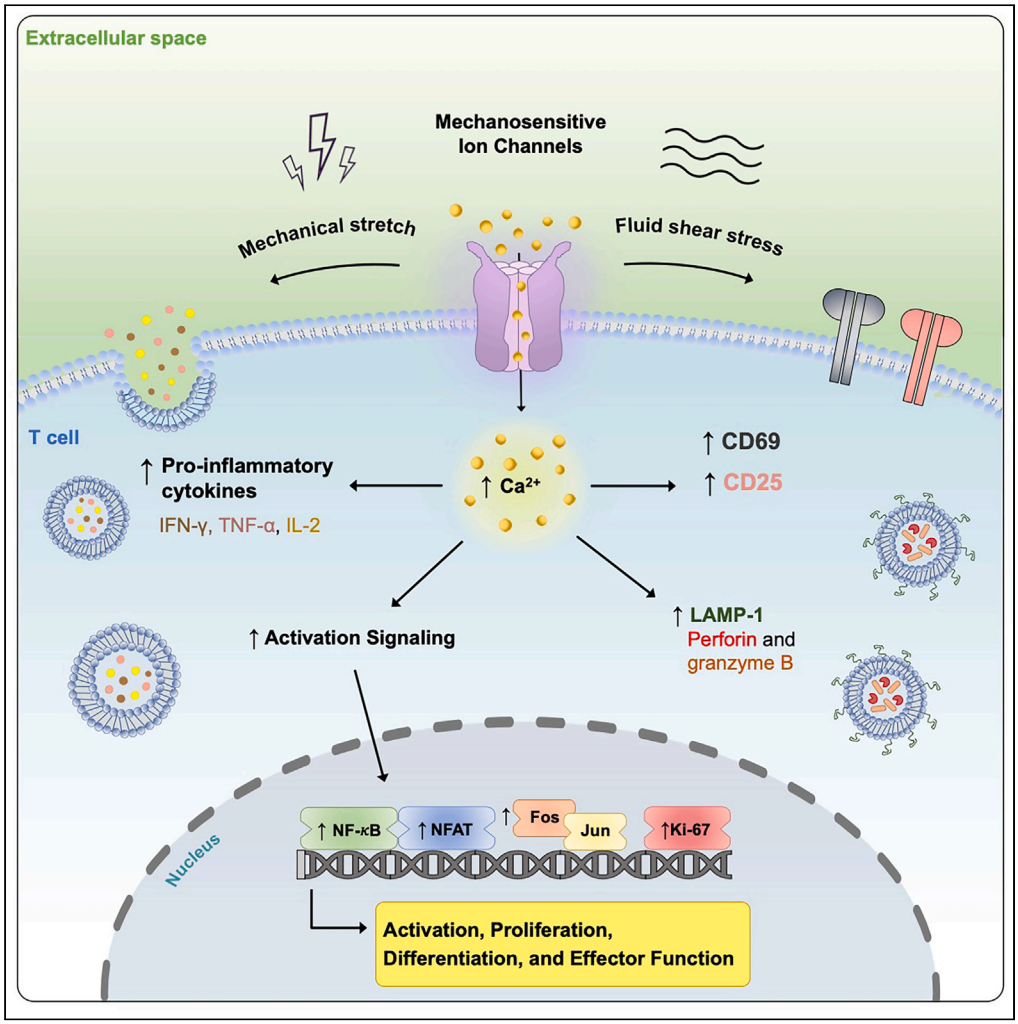

Nicole S. Sarna, Shanay H. Desai, Benjamin G. Kaufman, Natalie M. Curry, Anne M. Hanna, Michael R. King

mike.king@rice.edu

Highlights

Fluid shear stress (FSS) induces sustained T cell reprogramming over 10 days

FSS exposure enhances primary T cell activation, proliferation, and cytotoxicity

FSS + CD3/CD28 antibody synergy is mediated by mechanosensitive calcium ion channels

Sarna et al., iScience 27, 109999
June 21, 2024
https://doi.org/10.1016/j.isci.2024.109999

iScience

CellPress
OPEN ACCESS

Article

Enhanced and sustained T cell activation in response to fluid shear stress

Nicole S. Sarna,[1] Shanay H. Desai,[1,2] Benjamin G. Kaufman,[1] Natalie M. Curry,[1] Anne M. Hanna,[1] and Michael R. King[1,3,*]

SUMMARY

The efficacy of T cell therapies in treating solid tumors is limited by poor *in vivo* persistence, proliferation, and cytotoxicity, which can be attributed to limited and variable *ex vivo* activation. Herein, we present a 10-day kinetic profile of T cells subjected to fluid shear stress (FSS) *ex vivo*, with and without stimulation utilizing bead-conjugated anti-CD3/CD28 antibodies. We demonstrate that mechanical stimulation via FSS combined with bead-bound anti-CD3/CD28 antibodies yields a synergistic effect, resulting in amplified and sustained downstream signaling (NF-κB, c-Fos, and NFAT), expression of activation markers (CD69 and CD25), proliferation and production of pro-inflammatory cytokines (IFN-γ, TNF-α, and IL-2). This study represents the first characterization of the dynamic response of primary T cells to FSS. Collectively, our findings underscore the critical role of mechanosensitive ion channel-mediated mechanobiological signaling in T cell activation and fitness, enabling the development of strategies to address the current challenges associated with poor immunotherapy outcomes.

INTRODUCTION

Immunotherapy has revolutionized cancer treatments by stimulating a patient's immune system to enhance the anti-tumor response. Adoptive T cell transfer (ACT) involves the *ex vivo* manipulation of patient T cells and holds promise for treating a variety of diseases, with remarkable success observed in treating hematological cancers.[1] Despite the clinical advancements of ACT, a significant proportion of patients, particularly those with solid tumors, still experience disease progression.[2,3] While ongoing research aims to elucidate the precise mechanisms associated with disease progression, poor T cell cytotoxicity and persistence *in vivo* largely stem from inadequate T cell activation *ex vivo*.[4] While the most common approach used for *ex vivo* T cell activation is through the use of CD3/CD28 antibody-coated paramagnetic beads (αCD3/CD28), these are costly, have low throughput, and often fail to sufficiently activate immunocompromised cancer patient T cells.[5,6] Understanding the mechanisms in which optimal T cell activation can be achieved is critical to improving therapeutic outcomes for the treatment of solid tumors.

Significant strides have been made to enhance the effectiveness of T cell-based therapies by targeting biochemical signaling pathways. However, it is becoming increasingly evident that mechanical forces play a pivotal role in regulating immune cell activation and function.[7–11] Piezo1, a mechanosensitive ion channel, transduces physical stimuli into biochemical signals, where cell membrane deformation induced by fluid shear stress (FSS) results in calcium influx. Calcium serves as a universal second messenger in cell signaling and has a well-established role as a key regulator of T cell biology, due to its influence on T cell activation, proliferation, differentiation, and cytotoxic effector functions.[12,13]

Our group has recently discovered that constant and uniform mechanical stimulation of Piezo1 via FSS enhances the activation of T cells.[14] We demonstrated that this increase in T cell activation was dependent on Piezo1-mediated calcium signaling, determined by the pharmacological inhibitor of mechanosensitive ion channels (MSCs), GsMTX-4, and CRISPR-Cas9 knockout of Piezo1.[14] For decades, it has been recognized that a constant calcium stimulus must be maintained for 30–60 min for T cells to irreversibly commit to activation and proliferation, whereas an oscillatory calcium stimulus for the same duration fails to achieve this commitment.[15–20] This, in part, explains why the same activation is not achieved while in the blood circulation, where T cells encounter time-dependent shear forces that range from less than 1 dyn/cm^2 to magnitudes greater than 3,000 dyn/cm^2 in arterial bifurcations.[21,22] Therefore, there is a clear need to understand the fundamental response of T cells to mechanical forces and its impact on the complex T cell activation cascade.

This current study aimed to provide a 10-day kinetic profile of primary human T cell activation and function following a constant and uniform mechanical stimulation imposed within cone-and-plate viscometers. To our knowledge, this study represents the first attempt to characterize the dynamic T cell response to FSS for up to 10 days following activation. Collectively, we demonstrate that *ex vivo* T cell activation using αCD3/CD28 coupled with a continuous mechanical stimulation for 1 h yields a synergistic effect, substantially enhancing and maintaining T cell activation and fitness.

[1]Department of Biomedical Engineering, Vanderbilt University, 2301 Vanderbilt Place, Nashville, TN 37235, United States
[2]Department of Neuroscience, Vanderbilt University, 2301 Vanderbilt Place, Nashville, TN 37235, United States
[3]Lead contact
*Correspondence: mike.king@rice.edu
https://doi.org/10.1016/j.isci.2024.109999

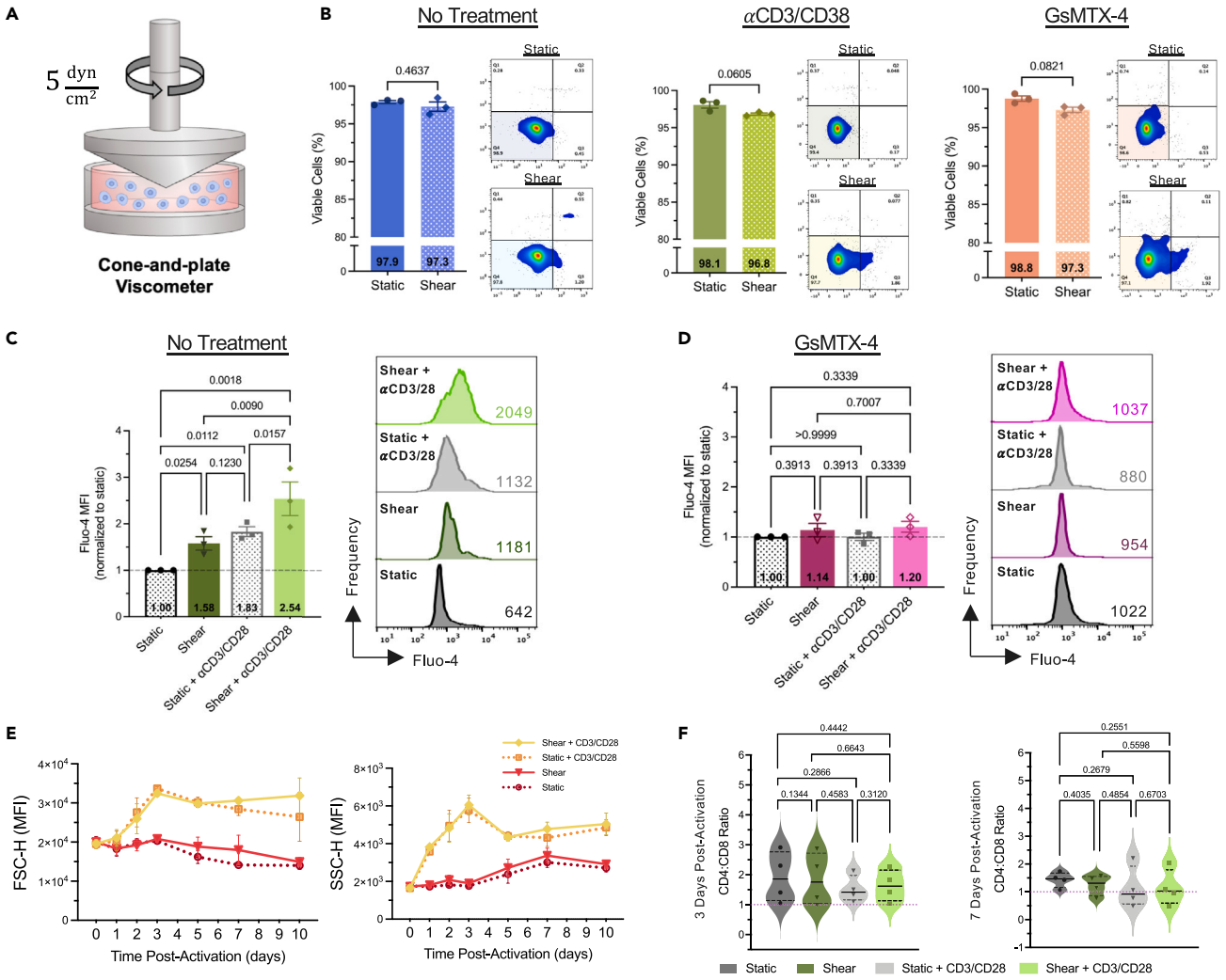

Figure 1. Stimulation with FSS in cone-and-plate viscometers induces MSC-mediated calcium influx and does not compromise T cell viability

(A) Schematic of cone-and-plate viscometer used to apply FSS treatments.

(B) Annexin V/Propidium Iodide (AV/PI) flow cytometry assay of T cells exposed to 5 dyn/cm^2 FSS for 1 h in cone-and-plate viscometers (500,000 cells/mL) with no treatment, with αCD3/CD28 beads, and with GsMTX-4. Data are presented as the percentage of viable cells (AV^-/PI^-) alongside representative flow cytometry plots. (N = 3; paired t test, two-tailed, α = 0.05).

(C and D) Intracellular calcium measured immediately (0 days) post activation via flow cytometry in the (C) absence and (D) presence of GsMTX-4. Data are presented as Fluo-4 MFI relative to static control T cells (N = 3, repeated measures (RM)-one-way ANOVA, α = 0.05) and representative flow cytometry plots of Fluo-4 fluorescence (presented with raw MFI).

(E) MFI of forward scatter (FSC-H) and side scatter (SSC-H) measured via flow cytometry in T cells 0–10 days post-activation (day 0, 2, 5, 7: N = 4, day 1: N = 3; day 3, 10: N = 5).

(F) CD4/CD8 ratio of T cells 3 days and 7 days post-activation treatments (N = 4; two-tailed ratio paired t test, α = 0.05, violin plots represent the mean as a solid line and first and third quartiles as dashed lines). Data represent the mean ± SEM unless otherwise stated, of T cells from N independent experiments, where each point within a condition represents a unique donor. All data and statistical analysis related to this figure are provided in Table S1.

RESULTS

Mechanical stimulation of T cells in cone-and-plate viscometers induces MSC-mediated calcium influx and does not compromise T cell health

Primary human T cells were isolated from whole blood samples and subsequently stimulated with bead-bound CD3/CD28 antibodies (αCD3/CD28) in both the presence and absence of FSS. Exposure of T cells to FSS lasted for 1 h at 5 dyn/cm^2, where a constant and uniform shear stress is expected within the cone-and-plate viscometer (Figure 1A). Bead-bound αCD3/CD28 was maintained in T cell culture following collection from the cone-and-plate viscometer and for the entire duration of culture. Importantly, FSS exposure under these conditions

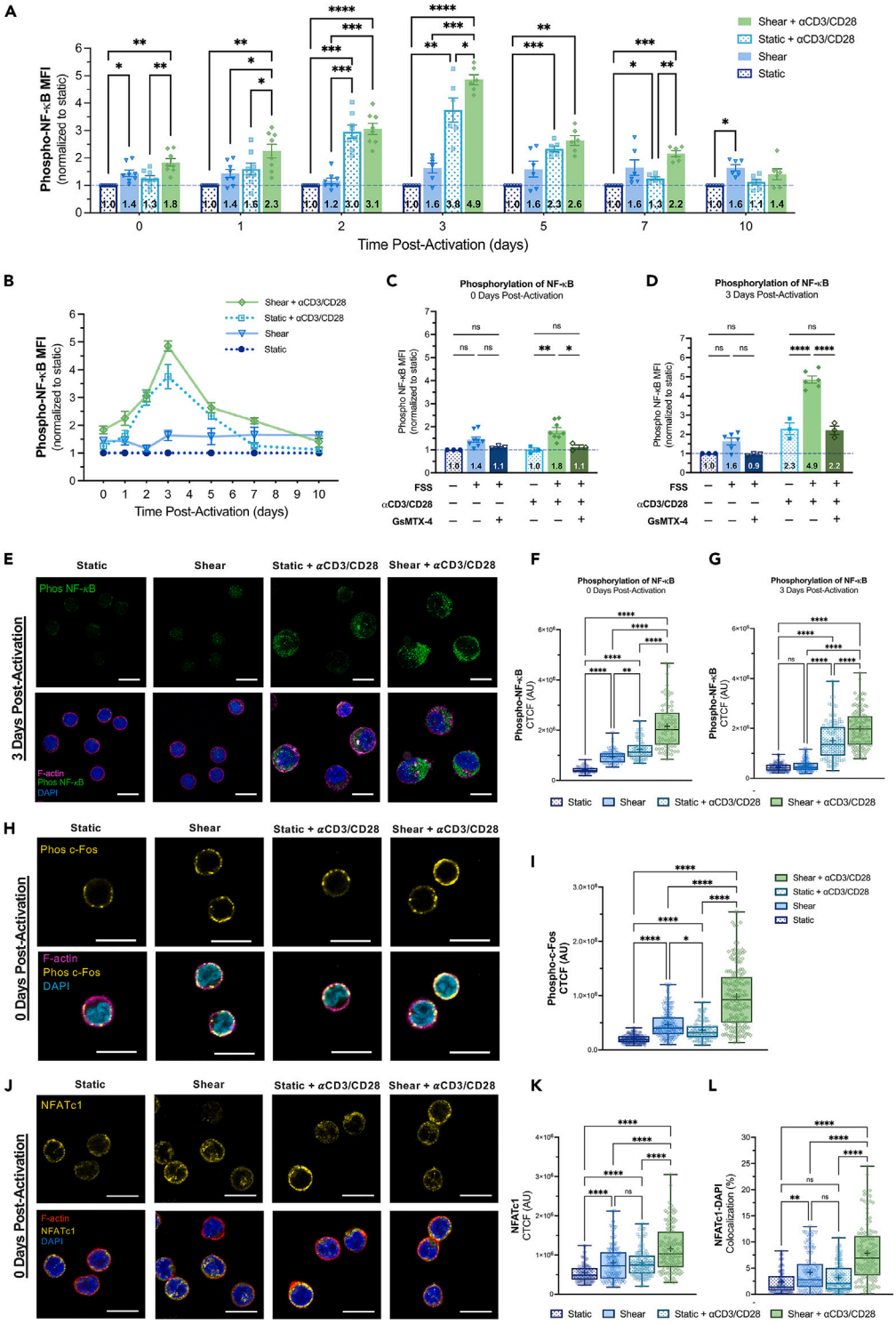

Figure 2. FSS in the presence and absence of CD3/CD28 antibody-coated beads enhances and sustains the phosphorylation of key activation proteins

(A and B) Phosphorylation of NF-κB MFI (relative to static control T cells) at 0–10 days post-activation via flow cytometry.

(C and D) Phosphorylation of NF-κB MFI (relative to static control T cells) at (C) 0 days and (D) 3 days post-activation with sheared conditions treated with GsMTX-4 where indicated. FSS conditions without GsMTX-4 are the same points shown in A and B and are included for clarity.

Figure 2. *Continued*

(E) Representative confocal images of the phosphorylation of NF-κB 3 days post-activation (phos-NF-κB = green; F-actin = magenta; DAPI = blue).

(F and G) Quantitative analysis of the phosphorylation of NF-κB (F) 0 days and (G) 3 days post-activation via confocal microscopy (0 days: $N = 2$, n = 75; 3 days: $N = 3$, n = 115) (H and I). Representative (H) confocal images and (I) quantitative analysis of the phosphorylation of c-Fos immediately (0 days) post-activation ($N = 3$, $n = 175$; phos-c-Fos = yellow; F-actin = magenta; DAPI = cyan).

(J–L) Representative (J) confocal images and quantitative analysis of (K) nuclear NFATc1 immunofluorescence and (L) NFATc1-DAPI colocalization (%) immediately (0 days) post-activation ($N = 3$, $n = 120$; NFATc1 = yellow; F-actin = red; DAPI = blue). (A–D) Data represent the mean ± SEM of T cells where each point within a condition represents a unique donor. Mean MFI are presented within each bar. Statistics calculated by (A and B) RM one- or (C and D) two-way ANOVA ($\alpha = 0.05$) and Tukey's multiple comparisons post-hoc test. (F, G, I, K, L) Boxplots expressing the median (central line), mean (plus symbol), first and third quartiles (bounds of box), and the highest and lowest values (whiskers), where N = independent experiments and n = total cells analyzed per condition. Statistics calculated by ordinary one-way ANOVA ($\alpha = 0.05$). (E, H, J) Scale bar, 10 μm *$p < 0.05$, **$p < 0.01$, ***$p < 0.001$, ****$p < 0.0001$. All data and statistical analysis related to this figure are provided in Table S2.

did not compromise T cell viability when shearing with αCD3/CD28 beads, GsMTX-4 treatment, or varying T cell concentrations of 250,000–750,000 cells/mL, as determined by an Annexin V-propidium iodide assay in flow cytometry (Figures 1B and S1).

The experimental conditions of this study incorporated static and FSS conditions in the presence (stimulated) and absence (unstimulated) of αCD3/CD28 beads. The static T cell conditions were subjected to the same environment and introduced to the viscometers without engaging rotation of the cone spindle. To evaluate the effect of mechanical stimulation of MSCs via FSS, Fluo-4 was used to quantify levels of intracellular calcium ($[Ca^{2+}]_i$) in flow cytometry (Figure 1C). Immediately following activation, a significant increase in $[Ca^{2+}]_i$ was observed for the FSS condition (1.58-fold change relative to static). Additionally, stimulation with αCD3/CD28 beads under static conditions induced a significant increase in $[Ca^{2+}]_i$, a well-documented early event resulting from T cell receptor (TCR)-crosslinking.[15,23,24] Notably, the combined application of FSS and αCD3/CD28 yielded a synergistic effect, with a statistically significant increase in $[Ca^{2+}]_i$ (2.54-fold change relative to static) compared to αCD3/CD28 alone (1.83-fold change relative to static). When MSCs were inhibited under shear conditions with GsMTX-4, a chemical inhibitor of MSCs,[25] the previously observed elevation in $[Ca^{2+}]_i$ due to FSS stimulation was eliminated (Figure 1D).

Upon activation, T cells undergo a blastogenic transformation, a process characterized by a 2- to 4-fold increase in cell volume to accommodate increased DNA synthesis and protein phosphorylation.[26,27] To assess these changes, the T cell size and intracellular complexity were quantified over a 10-day period, spanning from immediately post-activation to 10 days post-activation. This quantification was performed in flow cytometry using the forward scatter (FSC) and side scatter (SSC) parameters, respectively (Figure 1E). As others have previously reported,[26,28,29] a 3-way ANOVA revealed that T cells stimulated with αCD3/CD28 beads exhibited a substantial increase in both FSC and SSC, accounting for 35.17% and 39.36% of the total variation in FSC ($p < 0.0001$) and SSC ($p < 0.0001$) measurements, respectively (Table S1). The impact of FSS also yielded a statistically significant, albeit small effect, contributing to 0.3605% and 0.2705% of the total variation for FSC ($p = 0.0449$) and SSC ($p = 0.0034$), respectively. Furthermore, the interaction between αCD3/CD28 stimulation and time resulted in a significant impact on FSC ($p = 0.3100$) and SSC ($p = 0.0001$), indicating a highly dynamic FSC and SSC response to αCD3/CD28 stimulation over time. In contrast, interactions between FSS and time did not significantly affect FSC ($p = 0.0668$) and SSC ($p = 0.4939$), indicating that the statistically significant FSS-induced variations in FSC and SSC were constant and independent of time.

In addition, the ratio of $CD4^+$ and $CD8^+$ T cells was evaluated using flow cytometry at 3 and 7 days post-activation, where no significant differences were observed between any activation conditions (Figure 1F). The consistency in $CD4^+/CD8^+$ ratios suggests that although both αCD3/CD28 and mechanical stimulation influence the physical characteristics of T cells, they do not significantly affect the proportion of these T cell subsets at the studied time points. Together, these findings underscore the complex biophysical transformations that T cells undergo upon activation and the influence of mechanical stimulation in this process.

FSS in the presence and absence of αCD3/CD28 beads enhances and sustains the phosphorylation of key activation proteins

Given that increased cell size and complexity is indicative of heightened intracellular signaling activities, we investigated the impact of FSS on nuclear factor κB (NF-κB), an essential regulator of T cell activation, survival, and homeostasis.[30,31] Phosphorylation of NF-κB (phospho-NF-κB) was evaluated by flow cytometry for a period of 10 days (Figures 2A and 2B). Immediately post activation (0 days), both the FSS (1.44-fold change relative to static) and αCD3/CD28+FSS (1.83-fold change relative to static) T cells exhibited an increase in phospho-NF-κB. In contrast, aCD3/CD28 simulation alone dropped below both FSS conditions (1.25-fold change relative to static). The peak phospho-NF-κB signaling for all conditions was observed at 3 days post-activation, where αCD3/CD28+FSS T cells exhibited the highest increase (4.85-fold change relative to static) and surpassed stimulation with αCD3/CD28 under static conditions (3.75-fold change relative to static). By day 7, phospho-NF-κB was sustained in the αCD3/CD28+FSS condition (2.16-fold change relative to static), while nearly eliminated in the αCD3/CD28 condition (1.26-fold change relative to static). When MSCs were inhibited under FSS conditions, phospho-NF-κB at 0 days and 3 days post-activation (Figures 2C and 2D) was reduced, showing non-significant differences compared to their static counterparts. An additional experiment examined whether the heightened phospho-NF-κB response observed with αCD3/CD28+FSS was specifically due to the engagement of these receptors or if mechanical tension alone from beads bound to the cell surface could induce a similar effect. T cells subjected to FSS while conjugated to paramagnetic beads coated with αCD45 exhibited fold changes of 1.25 immediately after and 1.37 at day 3 post-FSS (Figure S2A), comparable to the increase observed with FSS without beads at the same time points (1.44-fold and 1.63-fold, respectively). These

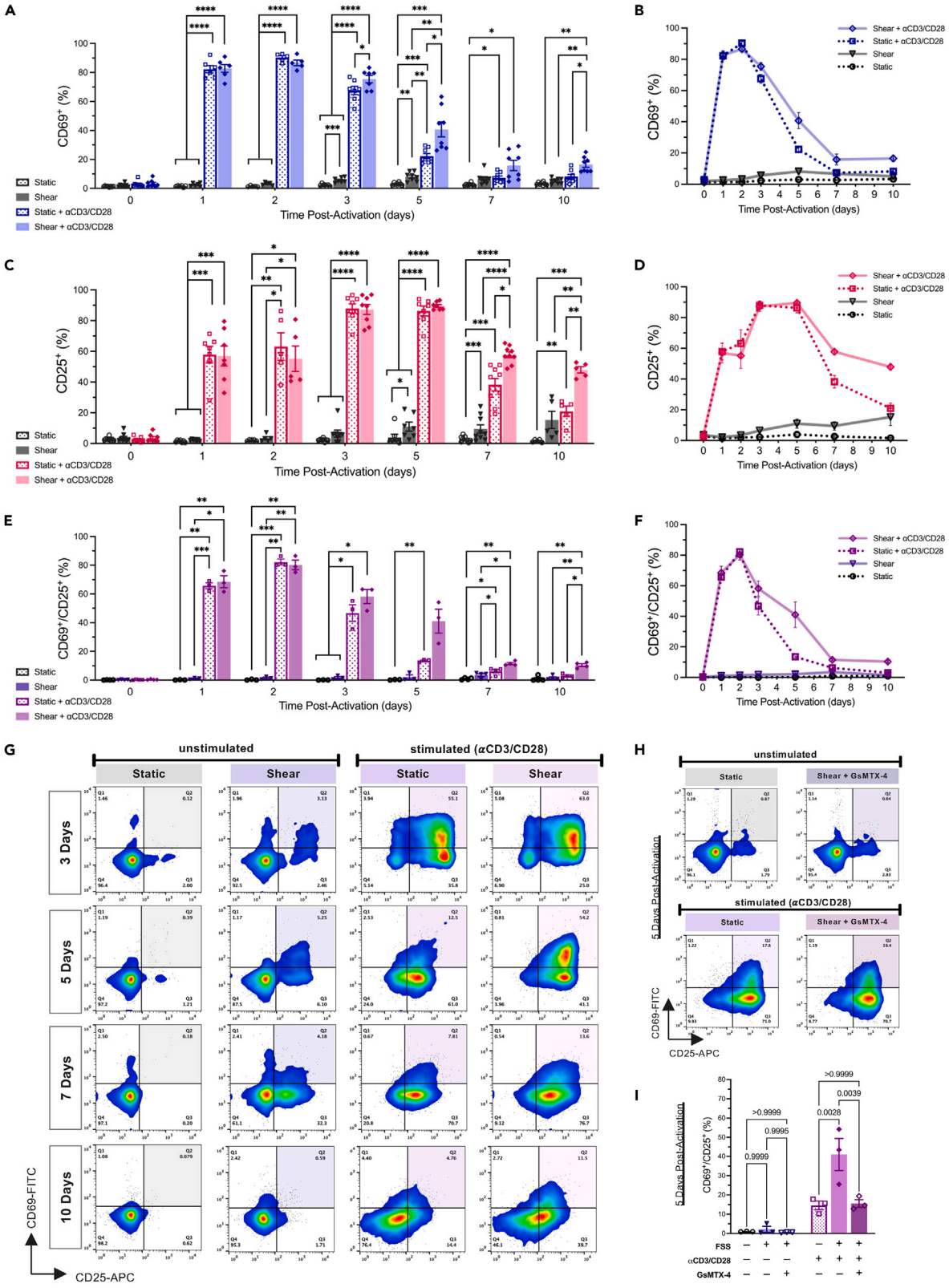
A
CD69⁺ (%)
Static
Shear
Static + αCD3/CD28
Shear + αCD3/CD28
Time Post-Activation (days)
B
CD69⁺ (%)
Shear + αCD3/CD28
Static + αCD3/CD28
Shear
Static
Time Post-Activation (days)
C
CD25⁺ (%)
Static
Shear
Static + αCD3/CD28
Shear + αCD3/CD28
Time Post-Activation (days)
D
CD25⁺ (%)
Shear + αCD3/CD28
Static + αCD3/CD28
Shear
Static
Time Post-Activation (days)
E
CD69⁺/CD25⁺ (%)
Static
Shear
Static + αCD3/CD28
Shear + αCD3/CD28
Time Post-Activation (days)
F
CD69⁺/CD25⁺ (%)
Shear + αCD3/CD28
Static + αCD3/CD28
Shear
Static
Time Post-Activation (days)
G
unstimulated
stimulated (αCD3/CD28)
Static
Shear
3 Days
5 Days
7 Days
10 Days
CD69-FITC
CD25-APC
H
unstimulated
Static
Shear + GsMTX-4
5 Days Post-Activation
stimulated (αCD3/CD28)
CD69-FITC
CD25-APC
I
5 Days Post-Activation
CD69⁺/CD25⁺ (%)
>0.9999
0.9995
0.9999
>0.9999
0.0039
0.0028
FSS
αCD3/CD28
GsMTX-4

Figure 3. FSS in the presence of anti-CD3/CD28 antibody-coated beads enhances and sustains the expression of T cell activation markers CD69 and CD25

(A and B) Percentage of T cells expressing CD69 at 0–10 days post-activation via flow cytometry.

(C and D) Percentage of T cells expressing CD25 at 0–10 days post-activation via flow cytometry.

(E and F) Percentage of T cells co-expressing CD69 and CD25 at 0–10 days post-activation via flow cytometry.

(G) Representative flow cytometry plots of CD69 and CD25 expression at 3, 5, 7, and 10 days post-activation.

(H and I) Representative (H) flow cytometry plots and (I) quantification of CD69 and CD25 co-expression at 5 days post-activation with sheared conditions treated with GsMTX-4 were indicated. (A–F) Data represent the mean ± SEM of T cells where each point within a condition represents a unique donor. Statistics calculated by RM-two-way ANOVA ($\alpha = 0.05$) and Tukey's multiple comparisons post hoc test. *$p < 0.05$, **$p < 0.01$, ***$p < 0.001$, ****$p < 0.0001$. All data and statistical analysis related to this figure are provided in Table S3.

findings suggest that the significant increase of phospho-NF-κB signaling in the αCD3/CD28+FSS condition is contingent upon specific ligand-receptor interactions, confirming the necessity of TCR-crosslinking with CD3/CD28.

To visualize phospho-NF-κB signaling in T cells, confocal microscopy was employed 0 and 3 days post-activation (Figures 2E–2G). A MATLAB algorithm (detailed in the method details section, "*CellAnalysis.m*") was created to quantify cell area and the corrected total cell fluorescence (CTCF) of phospho-NF-κB and F-actin. Confocal image analysis was consistent with flow cytometry results, where the αCD3/CD28+FSS condition exhibited the most significant increase in phospho-NF-κB at 0 and 3 days post-activation. Furthermore, stimulation with αCD3/CD28 under static and FSS conditions significantly increased cell area compared to the unstimulated T cells, further corroborating FSC results observed in flow cytometry (Figure S2B). The effect of FSS on F-actin polymerization dynamics has been well explored, albeit with various results.[32–35] The conflicting results between studies are likely associated with different cell types and FSS magnitude, duration, and method of FSS application. In this study, F-actin fluorescence intensity was significantly increased from the static control condition immediately following activation treatment. Interestingly, 3 days post-activation, F-actin decreased in both FSS-treated groups to a level comparable to the static control T cells, while the static αCD3/CD28 condition retained a statistically significant elevation in F-actin fluorescence (Figure S2C), suggesting a complex relationship between FSS and cytoskeletal dynamics. Additionally, we looked at the phosphorylation of c-Fos (phospho-c-Fos), which is a protein subunit that forms the activator protein-1 (AP-1) complex, immediately after activation treatments (Figures 2H, 2I, and S3). Immediately following activation treatment, phospho-c-Fos increased significantly compared to the static control T cells under all conditions, where FSS led to higher levels of phospho-c-Fos compared to the static αCD3/CD28 T cells. We also evaluated the translocation of NFATc1 into the nucleus imaged with confocal microscopy, where translocation was quantified using a MATLAB algorithm (detailed in the STAR Methods section, "*NuclearAnalysis.m*") that calculated the CTCF of NFATc1 immunofluorescence only within the nuclear stain (DAPI). NFATc1 translocation to the nucleus is a well-documented event that takes place within minutes after TCR-crosslinking and is directly dependent on calcium signaling.[23,36] Immediately after the 1 h activation treatments ("0 days"), we observed a significant increase in NFATc1 translocation into the nucleus, with the most significant increase observed in T cells stimulated with αCD3/CD28 under shear conditions (Figures 2J and 2K). Notably, FSS exposure significantly increased nuclear translocation of NFATc1 to a magnitude comparable to that observed in T cells stimulated with αCD3/CD28 under static conditions.

FSS in the presence of CD3/CD28 antibody-coated beads enhances and sustains the expression of T cell activation markers CD69 and CD25

Key indicators of T cell activation following TCR-crosslinking include the upregulation of surface markers CD69 and CD25.[37] The time course of this upregulation, following activation via αCD3/CD28-coated beads, has been well characterized, where CD69 is recognized as an early stage activation marker that is more immediate and short-lived compared to CD25, a later-stage activation marker. Thus, we evaluated the expression of CD69 and CD25 from 0 to 10 days post-activation using FSS in the presence and absence of αCD3/CD28 beads.

The rapid upregulation of $CD69^+$ first became evident in both the αCD3/CD28-stimulated groups, where the magnitude of the upregulation was similar for 1 and 2 days post-activation, at ∼82% and ∼90%, respectively (Figures 3A and 3B). Following the peak at 2 days post-activation, $CD69^+$ expression began to decline in both of the anti-CD3/CD28-stimulated groups. However, T cells activated by FSS maintained a significantly higher level of $CD69^+$ expression compared to all other activation conditions from day 3 to day 10 post-activation. In contrast, the static αCD3/CD28 condition had no statistically significant difference in $CD69^+$ expression on day 7 and day 10 post-activation, while the αCD3/CD28+FSS condition sustained significantly upregulated expression compared to all other activation conditions.

Furthermore, expression of late-stage $CD25^+$ increased at the same rate in both the static and FSS groups when stimulated with αCD3/CD28 beads, where expression was sustained at its peak for 3 and 5 days post-activation (Figures 3C and 3D). However, the αCD3/CD28 stimulation without FSS exposure displayed a rapid reduction in $CD25^+$ expression following its peak, which decreased to ∼38% and ∼21% of their initial expression at 7 and 10 days post-activation, respectively. In contrast, stimulation with αCD3/CD28+FSS resulted in a significantly higher expression of $CD25^+$, maintaining its expression ∼58% and ∼48% at 7 and 10 days post-activation, respectively. Of note, FSS exposure alone led to a significant increase in $CD25^+$ expression at 5, 7, and 10 days post-activation when compared to the static control T cells.

A flow cytometry panel of both antibodies was used to determine if co-expression of $CD69^+$ and $CD25^+$ was sustained (Figures 3E–3G). The double-positive $CD69^+/CD25^+$ expression peaked 2 days post-activation under both static and FSS-stimulated conditions. While T cells stimulated solely with αCD3/CD28 decreased $CD69^+/CD25^+$ to ∼14% by 5 days post-activation, the combined αCD3/CD28+FSS T cells sustained ∼41% double-positive population. Furthermore, when compared to the static control, the αCD3/CD28+FSS condition maintained a

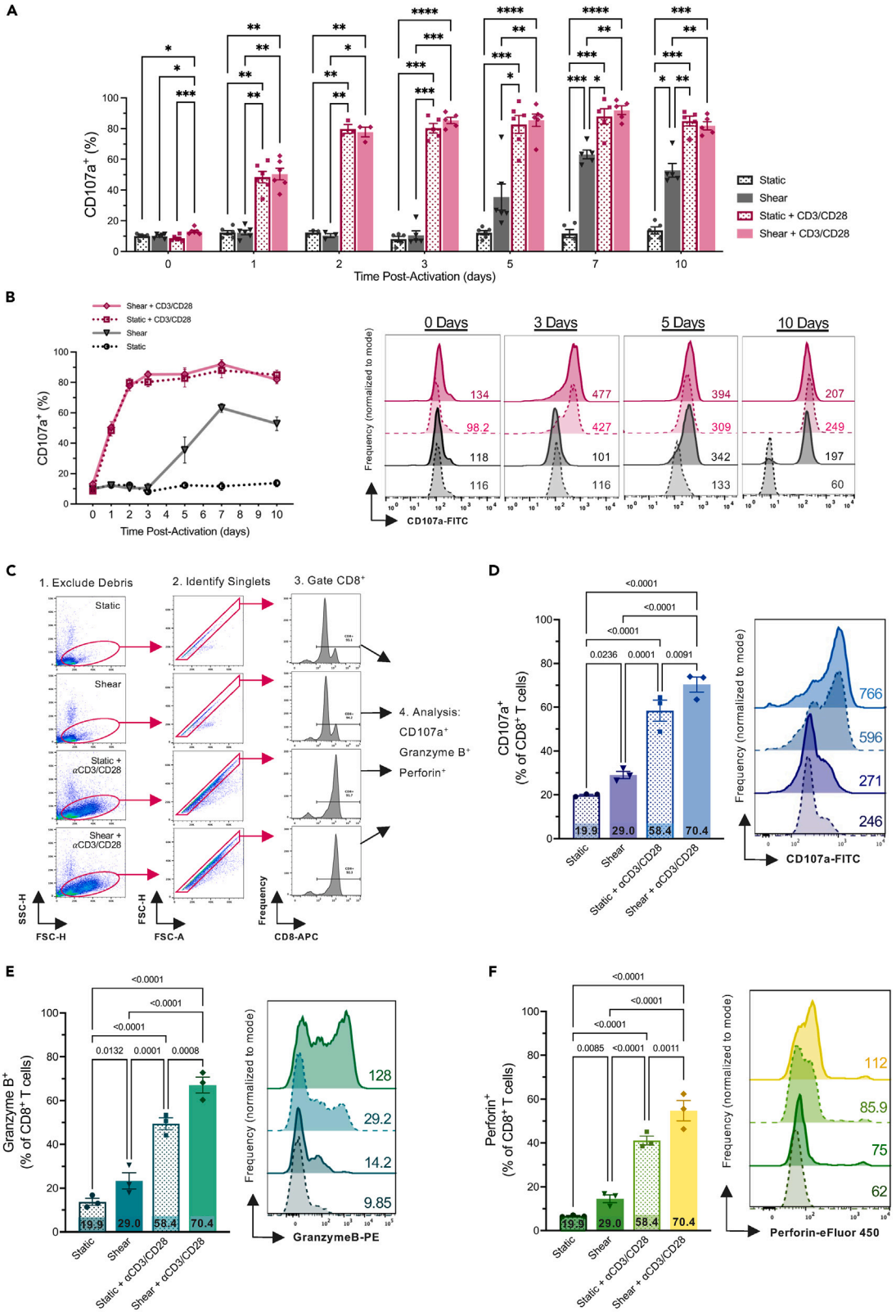
A
CD107a+ (%)
Time Post-Activation (days)
Static
Shear
Static + CD3/CD28
Shear + CD3/CD28
B
Shear + CD3/CD28
Static + CD3/CD28
Shear
Static
CD107a+ (%)
Time Post-Activation (days)
0 Days
3 Days
5 Days
10 Days
Frequency (normalized to mode)
CD107a-FITC
C
1. Exclude Debris
2. Identify Singlets
3. Gate CD8+
4. Analysis:
CD107a+
Granzyme B+
Perforin+
SSC-H
FSC-H
FSC-A
Frequency
CD8-APC
D
CD107a+ (% of CD8+ T cells)
Frequency (normalized to mode)
CD107a-FITC
E
Granzyme B+ (% of CD8+ T cells)
Frequency (normalized to mode)
GranzymeB-PE
F
Perforin+ (% of CD8+ T cells)
Frequency (normalized to mode)
Perforin-eFluor 450

Figure 4. FSS stimulation increases lytic granule production in Pan-CD4$^+$/CD8$^+$ and CD8$^+$-isolated primary T cells

(A and B) CD107a$^+$ percent expression 0–10 days post-activation via flow cytometry. Data represent the mean ± SEM of CD107a$^+$ in Pan-T cells isolated from unique donors (day 0, 1, 5: $N = 6$, day 3, 7, 10: $N = 5$, day 2: $N = 3$; RM-two-way ANOVA, $\alpha = 0.05$). Representative flow cytometry plots of CD107a$^+$ expression at 0, 3, 5, and 10 days post-activation relative to static control T cells (presented with raw MFI).

(C) Flow cytometry gating strategy for isolated CD8$^+$ T cells.

(D–F) CD8$^+$ T cells evaluated in flow cytometry for (D) CD107a$^+$, (E) granzyme B$^+$, and (F) perforin$^+$ at 3 days post-activation. Data represent the mean ± SEM and representative flow cytometry plots (presented with raw MFI) of CD8$^+$ T cells isolated through magnetic separation from 3 unique donors ($N = 3$; RM-two-way ANOVA, $\alpha = 0.05$). *$p < 0.05$, **$p < 0.01$, ***$p < 0.001$, ****$p < 0.0001$. All source data and statistical analysis related to this figure are provided in Table S4.

significantly higher CD69$^+$/CD25$^+$ expression of ~10.5% at 7 and 10 days post-activation. To further validate these findings, when Piezo1 function was inhibited with GsMTX-4 in the FSS conditions, no significant difference was observed in the percentage of CD69$^+$/CD25$^+$ populations 5 days post-activation (Figures 3H and 3I).

FSS stimulation increases lytic granule production in Pan-CD4$^+$/CD8$^+$ and CD8$^+$-isolated primary T cells

The efficacy of T cell-based immunotherapies, particularly in the context of cancer immunotherapy, is critically dependent on the cytotoxic potential of adoptively transferred cells. To investigate the impact of FSS on T cell cytotoxicity, we evaluated CD107a$^+$ expression over a 10-day time period post-activation using flow cytometry. CD107a, also known as lysosomal-associated membrane protein-1, serves as a critical marker for degranulation and has been shown to indicate cytotoxic T cell function.[29,38] It is expressed on intracellular vesicles that contain lytic granzymes and perforins secreted by T cells to kill target cells. For T cells stimulated with αCD3/CD28, CD107a$^+$ expression was found to reach its peak at 7 days post-activation under static (~90%) and FSS (~93%) conditions (Figures 4A and 4B). Therefore, FSS had no significant impact on CD107a$^+$ expression when stimulated with αCD3/CD28 beads. Interestingly, at 5 days post-activation, T cells exposed solely to FSS exhibited an increase in CD107a$^+$ expression from 10%–12% at 0–3 days post-activation to ~36%, ~69%, and 53% at days 5, 7, and 10 post-activation.

Since a number of T cell immunotherapies focus on the adoptive transfer of cytotoxic CD8$^+$ T cells to eradicate tumor cells, we evaluated the cytotoxic potential of T cells isolated via CD8$^+$ magnetic separation 3 days post-activation. In addition to CD8$^+$-specific T cell isolation, only T cells expressing CD8 were evaluated by employing CD8$^+$ gating in the flow cytometry gating strategy (Figure 4C). CD8$^+$ T cells exposed to FSS with and without αCD3/CD28 elicited a significant upregulation in the expression of cytotoxic markers—CD107a, granzyme B, and perforin—compared to their static counterparts (Figures 4D and 4E). The application of FSS had the largest impact on granzyme B production in CD8$^+$ T cells. In the absence of αCD3/CD28, the application of FSS alone resulted in an increase in granzyme B, rising from 13.7% to 23.3%. This effect was even more pronounced in the presence of αCD3/CD28, where granzyme B expression increased from 49.4% under static conditions to 67.1% under FSS conditions. This trend was consistent for CD107a and perforin, where FSS application without αCD3/CD28 resulted in a ≥8% increase and a ≥12% increase with αCD3/CD28 stimulation for both cytotoxicity markers. These data suggest that mechanical stimulation of T cells alone increases cytotoxic potential, which can be further augmented with αCD3/CD28 beads.

FSS stimulation increases pro-inflammatory cytokine secretion

We also examined the secretion of pro-inflammatory cytokines, including IFN-γ, TNF-α, and IL-2, through an enzyme-linked immunosorbent (ELISA) assay and intracellular cytokine staining in flow cytometry. The ELISA was performed after collecting the media conditioned by cells at 3 days post-activation and demonstrates that FSS, particularly when combined with αCD3/CD28 stimulation, significantly increases the secretion of IFN-γ, TNF-α, and IL-2 (Figure 5A). Notably, stimulation with αCD3/CD28+FSS resulted in an average percent increase in IFN-γ, TNF-α, and IL-2 cytokine secretion by a magnitude of 248.4%, 148.3%, and 268.0%, respectively, when compared to the stimulation with αCD3/CD28 alone.

To evaluate cytokine production, a protein transport inhibitor (GolgiPlug) was incubated with T cells at 3 and 7 days post-activation for a total of 4 h to allow cytokines to accumulate within the cell. The median fluorescence intensity (MFI) was quantified in flow cytometry to determine intracellular cytokine production levels. At 3 days post-activation, T cells stimulated with αCD3/CD28+FSS exhibited the highest levels of cytokine production, resulting in an average percent increase (relative to static) of 506%, 401%, and 474% for secretion of IFN-γ, TNF-α, and IL-2, respectively (Figure 5B). In the absence of FSS, anti-CD3/CD28 stimulation only increased IFN-γ, TNF-α, and IL-2 secretion (relative to static) by 202%, 175%, and 191%, respectively. Most notably, T cells exposed solely to FSS exhibited an increase (relative to static) of 245%, 224%, and 261%, for IFN-γ, TNF-α, and IL-2, respectively—all of which were greater than the levels observed in T cells stimulated solely with anti-CD3/CD28 beads under static conditions. By 7 days post-activation, cytokine production in both static and shear αCD3/CD28 conditions attenuated below the static control, and T cells exposed to FSS exhibited only slightly higher cytokine production than the static control (Figure 5C).

It is important to note that while ELISA measures accumulated secreted cytokines in the culture medium, intracellular cytokine staining via flow cytometry quantifies cytokines retained within cells at a single point in time. The discrepancy between the two methods, namely in the pro-inflammatory cytokines measured in the FSS-only condition, is likely due to differences in the timing of secretion events and the cytokine dynamics (synthesis versus release). For instance, a higher MFI in flow cytometry does not necessarily translate to higher levels in the ELISA assay if the cytokines are retained within the cell. Conversely, ELISA may detect higher amounts of cytokines even if the intracellular levels measured by flow cytometry are lower, suggesting efficient secretion mechanisms. Nonetheless, these data indicate that FSS, particularly when stimulated with αCD3/CD28, significantly upregulates the production and secretion of key pro-inflammatory cytokines in primary T cells.

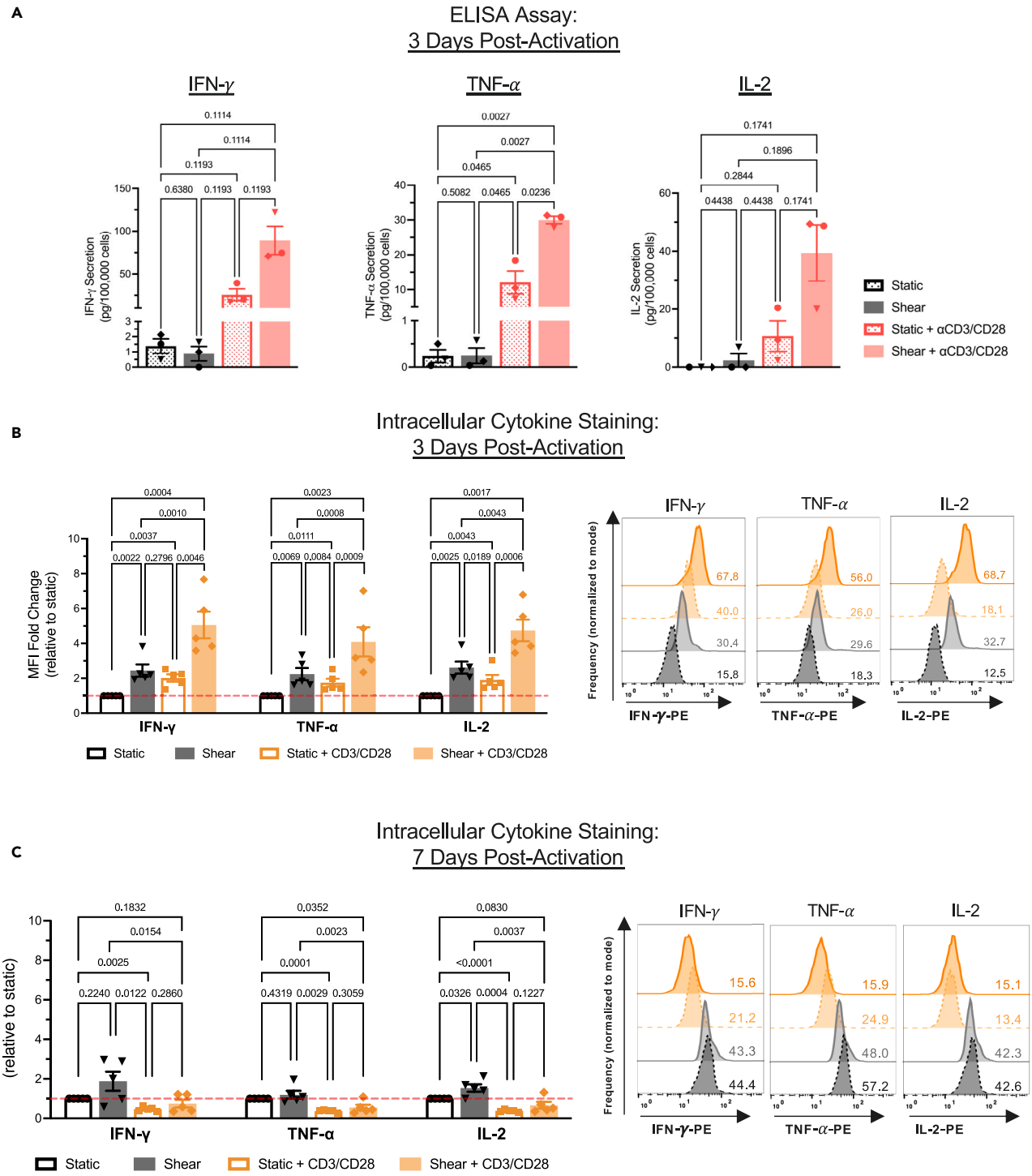

Figure 5. FSS stimulation increases pro-inflammatory cytokine production

(A) IFN-γ, TNF-α, and IL-2 quantified via ELISA assay 3 days post-activation. Cell-conditioned media was collected from cultured T cells and the quantified cytokine secretion was normalized to cell number at the time of supernatant collection. Data represent the mean ± SEM of IFN-γ, TNF-α, and IL-2 of T cells isolated from 3 different donors (N = 3; RM-two-way ANOVA, α = 0.05).

(B and C) IFN-γ, TNF-α, and IL-2 MFI (relative to static control T cells) measured in flow cytometry at (B) 3 and (C) 7 days post-activation. Data represent the mean ± SEM of IFN-γ, TNF-α, and IL-2 MFI of T cells isolated from 5 donors (N = 5; two-tailed ratio paired t test, α = 0.05). Representative flow cytometry plots are presented with raw MFI. Source data and statistical analyses are provided in Table S5.

Mechanical stimulation via FSS enhances T cell proliferation

Given the crucial role of calcium signaling in cell proliferation, we investigated the effect of mechanical stimulation of Piezo1 via FSS on T cell proliferation over 10 days. Cells were stained with a proliferation dye (VPD450) immediately after activation and cultured for 3 days prior to flow cytometry analysis. Anti-CD3/CD28 stimulation resulted in rapid expansion of T cells, which is consistent with prior studies, where the T cell doubling time was <24 h. In T cells activated with αCD3/CD28+FSS, ~80% of cells were undergoing cell division (presented as % proliferating), which was significantly higher compared to the ~65% proliferation observed when stimulated solely with anti-CD3/CD28 (Figures 6A and 6B). Furthermore, FSS exposure without anti-CD3/CD28 stimulation resulted in a significant increase in proliferating T cell populations when compared to static conditions. However, upon inhibition of MSCs with GsMTX-4, T cells stimulated with αCD3/CD28+FSS demonstrated only ~36% of proliferating cells, a significant decrease compared to the conditions in which MSCs were fully functional, whether under static or FSS-stimulated conditions. These findings emphasize that MSC function is required to facilitate robust T cell proliferation, irrespective of the presence or absence of αCD3/CD28 stimulation.

Proliferation was also assessed with Ki67 in flow cytometry (presented as % $Ki67^+$) over the 10 days post-activation period (Figures 6C and 6D). An increase in $Ki67^+$ was observed in both αCD3/CD28-stimulated groups that began 2 days post-activation and peaked 5 days post-activation. However, after 7 days post-activation, the percentage of cells positive for Ki67 decreased to ~13% and ~26% in T cells stimulated with αCD3/CD28 under static and FSS conditions, respectively.

To determine the extent of active Ki67 transcription, we used high magnification confocal microscopy to visualize nuclear Ki67 immunofluorescence (Figure 6E). Indicated by confocal microscopy analysis, there was a significant increase in the extent of nuclear Ki67 expression in T cells stimulated with both αCD3/CD28 and FSS compared to all other T cell conditions (Figures 6F and 6G).

DISCUSSION

In this study, we investigated the impact of constant and uniform mechanical stimulation on primary human T cell activation and function, in the context of developing novel strategies to improve *ex vivo* activation for a broad class of T cell-based applications such as ACT. The conventional approach to *ex vivo* T cell activation utilizes CD3/CD28 antibody-coated paramagnetic beads, as used in this study.[5] While this method is expensive, low-throughput, and elicits high intrapersonal variability, it is currently the most effective and feasible option for clinical settings.[5,6] We sought to gain a 10-day kinetic profile of T cell response to FSS in the presence and absence of bead-bound CD3/CD28, due to the dynamic nature of this process and the clinical relevance of T cell longevity for ACT. Our findings demonstrate that primary human T cells exposed to FSS for 1 h *ex vivo* lead to a sustained increase in activation and fitness, characteristic of pro-anti-tumor responses. Our findings, combined with previous observations, highlight the major role that mechanotransduction plays in influencing T cell behavior, offering significant implications for current and future *ex vivo* T cell manufacturing strategies.

The importance of calcium signaling in T cells is underscored by the fact that 75% of all T cell activation-regulated genes exhibit dependence on calcium.[39] Upon TCR-ligation, a spike in $[Ca^{2+}]_i$ occurs due to the release of Ca^{2+} from the endoplasmic reticulum (ER) Ca^{2+} stores. However, the initial $[Ca^{2+}]_i$ surge from the ER is small in magnitude, transient, and insufficient to drive gene expression.[40] The ER Ca^{2+} store depletion triggers store-operated Ca^{2+} entry (SOCE), taking place within minutes and producing oscillatory $[Ca^{2+}]_i$ dynamics.[40,41] It is well established that a prolonged calcium signal must be maintained for 30–60 min for T cells to commit to activation and proliferation.[15,16,20] As a mechanosensitive calcium ion channel, Piezo1 operates independently of SOCE, allowing passive calcium influx when activated by mechanical stimuli. Therefore, we investigated the effect of 1 h FSS exposure on T cells over the course of 10 days.

We first explored the early activation events following FSS exposure in the presence and absence of TCR stimulation by evaluating three prominent T cell activation transcription factors, including NF-κB, NFATc1, and c-Fos, which form the AP-1 complex.[42,43] NFAT translocation is exclusively dependent on cytosolic calcium, which subsequently activates calcineurin and facilitates its localization to the nucleus.[44] Here, we show that 1 h of FSS exposure without TCR stimulation induces NFATc1 translocation to a similar magnitude as T cells stimulated with anti-CD3/CD28 beads under static conditions. While the Ca^{2+}-/Calcineurin/NFAT pathway has been well defined, the role of Ca in the regulating NF-κB and AP-1 is less understood, especially considering the long-term dynamics.[23,24,37,45,46] We demonstrated that FSS combined with αCD3/CD28 beads results in the most pronounced effect compared to all other conditions, as T cells stimulated with αCD3/CD28 under FSS conditions exhibited the most significant increase in phospho-NF-κB, phospho-c-Fos, and NFATc1. Our results demonstrate that FSS modulates the magnitude of TCR response by amplifying signaling in the NF-κB, AP-1, and NFAT pathways.

Furthermore, the expression of CD69/CD25 was upregulated in conditions stimulated with αCD3/CD28 beads. Of note, when T cells were stimulated with αCD3/CD28 under FSS conditions, the individual expression and co-expression of CD69 and CD25 were sustained at levels higher than T cells stimulated with αCD3/CD28 beads under static conditions for 10 days. When Piezo1 was inhibited with GsMTX-4 for FSS conditions, the sustained co-expression observed at 5 days post-activation was no longer evident. These results suggest that FSS enhances TCR-mediated activation of T cells.

To further evaluate the T cell response to FSS, $CD107a^+$ expression was assessed via flow cytometry. Over the 10 day span, no significant differences were noted between the αCD3/CD28-stimulated conditions in the presence or absence of FSS in $CD107a^+$ upregulation. However, one of the surprising results of this study was the upregulation of $CD107a^+$ in T cells that were exposed solely to FSS 5, 7, and 10 days post-activation. Interestingly, the T cells exposed only to FSS exhibited this increase in $CD107a^+$ expression first observed 5 days post-activation, which aligns with the increase in cell size, as determined by FSC in flow cytometry. These findings suggest that FSS induces intracellular reprogramming that leads to modulated cellular function for up to 5 days post-activation.

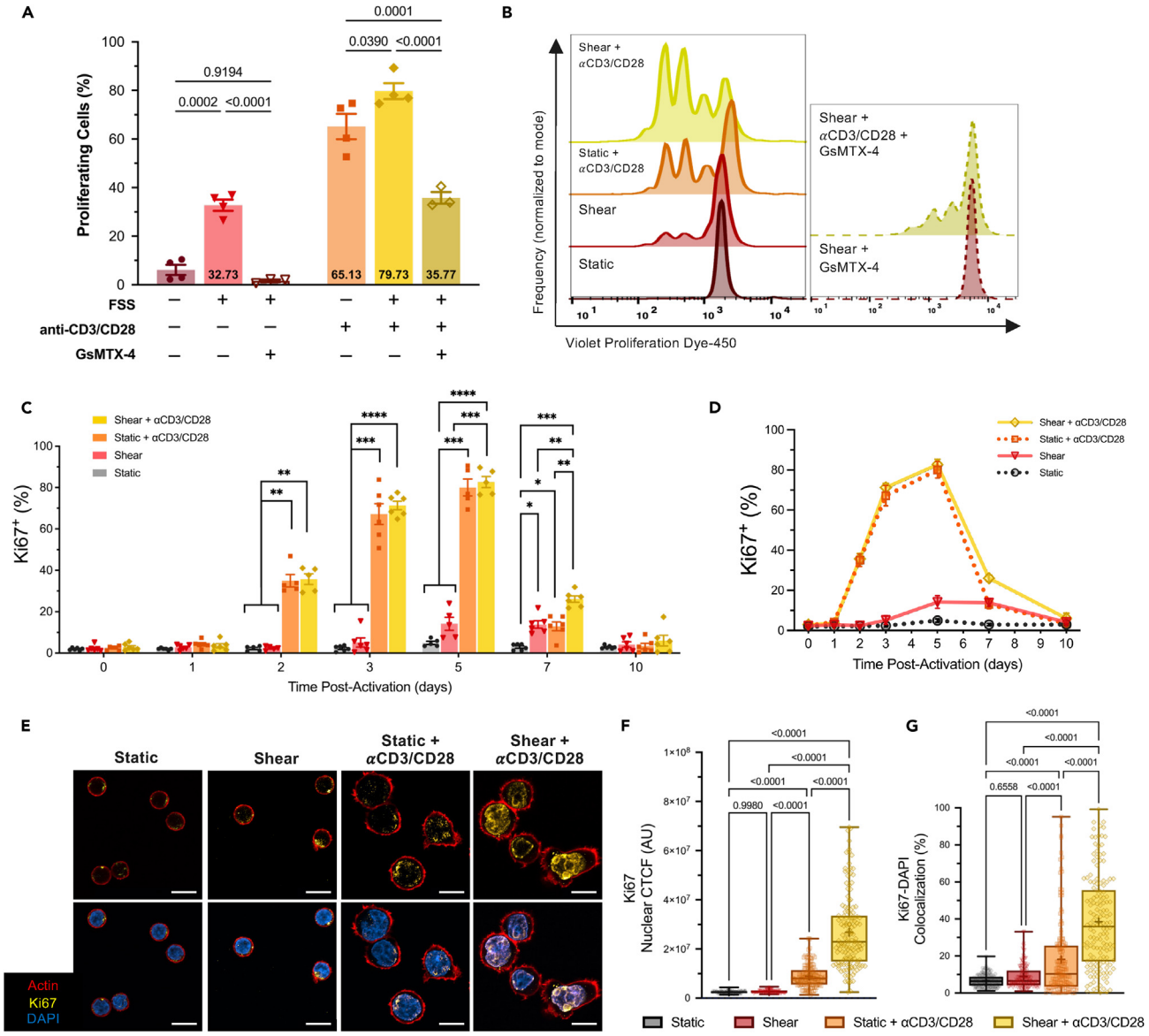

Figure 6. Mechanical stimulation via FSS enhances T cell proliferation

(A and B) Quantification of (A) proliferating cells (%) and (B) representative flow cytometry plots of violet proliferation dye (VPD450) at 3 days post-activation. Data represent the mean ± SEM of proliferating T cells isolated from 3 to 4 healthy donors, where the mean percentage is presented within the bars (Static, Shear, Static+αCD3/CD28, Shear+αCD3/CD28: $N = 4$; Shear+GsMTX-4, Shear+αCD3/CD28+GsMTX-4: $N = 3$; two-way ANOVA, $\alpha = 0.05$).

(C and D) Ki67$^+$ percent expression at 0–10 days post-activation via flow cytometry. Data represent the mean ± SEM of Ki67$^+$ expression in T cells isolated from 4 to 6 donors (day 0: $N = 6$, day 1: $N = 6$, day 2: $N = 5$, day 3: $N = 6$, day 5: $N = 5$, day 7: $N = 6$, day 10: $N = 6$; RM-two-way ANOVA, $\alpha = 0.05$).

(E) Representative confocal images of T cells 3 days post-activation (Ki67 = yellow; Actin = red; DAPI = blue). Scale bar, 10 μm.

(F and G) Quantitative analysis of confocal images representing (F) nuclear Ki67 immunofluorescence and (G) Ki67-DAPI colocalization (%) in T cells 3 days post-activation ($N = 3$, n = 150 per group; one-way ANOVA, $\alpha = 0.05$; Outliers removed, ROUT Method, Q = 1%). Boxplots expressing the median (central line), mean (plus symbol), first and third quartiles (bounds of box), and the highest and lowest values (whiskers), where N = independent experiments and n = total cells analyzed per condition. *$p < 0.05$, **$p < 0.01$, ***$p < 0.001$, ****$p < 0.0001$. All data and statistical analysis related to this figure are provided in Table S6.

In addition, we demonstrated that T cells stimulated with FSS and αCD3/CD28 beads result in a significant increase in pro-inflammatory cytokine production and secretion 3 days post-stimulation. The increased intracellular cytokine content (as measured via flow cytometry) and augmented cytokine secretion (as measured via ELISA assay) confirm that mechanical stimuli can substantially enhance the inflammatory potential of T cells. These data have significant implications for the design and optimization of T cell-based immunotherapies, as previous studies have linked the presence of these pro-inflammatory cytokines with favorable outcomes in cancer therapies and their potential for exhibiting anti-tumor effects.[47,48] The observed differences between the ELISA and intracellular cytokine staining for the FSS-alone

condition underscore the complexity of cytokine regulation and the need for complementary approaches to fully understand cytokine dynamics.

Notably, an experimental design choice for the present study involved culturing T cells without cytokine supplements. This approach enabled the evaluation of the isolated effects of FSS on T cell functionality to elucidate effects that may be attributed to cytokine supplementation and prevent polarization toward a specific T cell subset. Moreover, this is particularly relevant when considering the "cold" tumor microenvironment, which is characterized by a lack or absence of inflammatory and stimulating cytokines. This suggests that the *ex vivo* stimulation of T cells with FSS might be further augmented by the addition of cytokine supplements.

While cytokine storm is a warranted consideration when considering the extent of T cell activation for ACT, numerous studies have explored the myriad of factors involved with cytokine storm, including age, disease type, and extent of disease. Studies have shown that T cells obtained from patients with late-stage disease exhibit a significantly higher activation threshold when stimulated with CD3/CD28 antibodies (soluble or bead-bound), primarily due to T cell exhaustion. Furthermore, the low activation capacity observed in T cells from late-stage disease patients is likely a reason why ACT therapies fail in the clinic, as it leads to low cytotoxicity, proliferation, and persistence *in vivo*. The present work suggests that mechanical stimulation may be used to lower the threshold of activation of T cells during *ex vivo* manipulation for patients with advanced disease. Preliminary data in our lab support this idea, where stage 4 cancer patient samples demonstrate an even greater response to FSS stimulation alone when compared to the αCD3/CD28 alone (data not shown). Therefore, a better understanding of the mechanism that underlies the mechanical sensitization to T cell activation would enable optimization of the *ex vivo* activation process to maximize anti-tumor effect while reducing the risk of cytokine storm.

Calcium is a key regulator of cell proliferation, and its absence can drastically hinder the proliferative capacity of various cell types. To investigate the impact of Piezo1 activation and subsequent calcium influx on proliferation, a violet proliferation dye (VPD450) was used to track active cell division. We found that exposure to FSS alone induced a modest increase in proliferating cells 3 days post-activation to 32.73%, while stimulation with αCD3/CD28 increased this to 65.13% under static conditions and 79.73% when exposed to FSS. We then evaluated proliferation based on the percentage of $Ki67^+$ cells in flow cytometry. Both αCD3/CD28 and αCD3/CD28+FSS conditions increased $Ki67^+$ expression to the same degree, beginning at 2 days and peaking at 5 days post-activation. To gain a better understanding of the extent of active Ki67 transcription, we used confocal microscopy and a MATLAB algorithm to quantify the fluorescence of nuclear Ki67 3 days post-activation. In contrast to the percentage of $Ki67^+$ cells determined by flow cytometry, confocal image analysis revealed a significantly higher Ki67 fluorescence in the nucleus in the αCD3/CD28 samples stimulated with FSS exposure, surpassing all other activation conditions. This indicates that the combination of αCD3/CD28 stimulation combined with FSS exposure greatly augments a T cell's capacity for proliferation.

While this study did not explore the effects of FSS on T cell differentiation or the modulation of specific T cell subsets, our lab has previously demonstrated that both mechanical and chemical stimulation of Piezo1, via FSS and Yoda1, respectively, enhances activation of $CD4^+$ and $CD8^+$ T cells in combination with soluble or bead-bound CD3/CD28 antibodies.[14] It has also been observed that Piezo1-deficient $CD4^+$ and $CD8^+$ T cells exhibit diminished priming capacity by allogenic monocytes, failing to achieve full activation due to impaired TCR-crosslinking.[49] Another group demonstrated that loss of Piezo1 in T cells selectively enhances T_{reg} expansion and function, which mitigated disease severity in an animal model for experimental autoimmune encephalomyelitis.[50] While the present study used GsMTX-4 to inhibit MSCs rather than genetic manipulation of individual protein channels, GsMTX-4 is a specific inhibitor of cationic MSCs belonging to the Piezo1 and transient receptor potential (TRP) protein families.[25,51,52] Importantly, it has been shown that TRP channels, including TRPV4 and TRPC6, fail to respond to mechanical stretch activation or mechanical force imposed by fluid shear stresses, suggesting minimal involvement of TRP channels in the present study.[53] Therefore, our findings, along with prior research, suggest that Piezo1 activation and function in T cells are pro-inflammatory and engages various T cell subsets, warranting the need for further investigation. Collectively, the growing body of research exploring the impact of mechanical forces via Piezo1 in T cells points to promising avenues for identifying targets for therapeutic interventions for a variety of diseases, including cancer, chronic inflammatory disorders, and hypertension. Our findings underscore potential strategies that utilize FSS to leverage T cell fitness, improve their sensitivity to antigens, and fine-tune immune responses to achieve better therapeutic outcomes.

Limitations of the study

As with any study, this work is not without limitations. Here, we have presented a comprehensive kinetic profile of T cell activation and function in response to FSS, both with and without stimulation from αCD3/CD28 beads. Our findings indicate that the augmented activation levels and cellular fitness in response to FSS is mediated through mechanosensitive calcium ion channels, and is inhibited by GsMTX-4. Nonetheless, further investigation into the exact mechanisms underlying this behavior is needed to determine the optimal magnitude and duration of FSS exposure. In addition, transcriptomic analyses of primary T cells subjected to FSS could enable the identification of genomic changes induced by mechanical stimulation. This approach could also provide valuable insights into the underlying mechanisms that contribute to differences in activation and functional capacity among healthy donor T cells.

STAR★METHODS

Detailed methods are provided in the online version of this paper and include the following:

- KEY RESOURCES TABLE

SUPPLEMENTAL INFORMATION

Supplemental information can be found online at https://doi.org/10.1016/j.isci.2024.109999.

ACKNOWLEDGMENTS

This work was supported by the National Institutes of Health, grant number R01CA256054 to M.R.K. This material is based on work supported under National Science Foundation Graduate Research Fellowship to N.S.S. (1937963). Funding from the SyBBURE Searle Undergraduate Research Program was provided to S.H.D. and N.S.S.

AUTHOR CONTRIBUTIONS

Conceptualization, M.R.K. and N.S.S.; formal analysis, N.S.S., S.H.D., B.G.K., and N.M.C.; investigation, N.S.S., S.H.D., B.G.K., N.M.C., and A.M.H.; writing (original draft), N.S.S.; writing (review and editing), M.R.K., S.H.D., and N.S.S.; funding acquisition, M.R.K.; supervision, M.R.K.

DECLARATION OF INTERESTS

The authors disclose a US Patent application related to this study, with M.R.K. and N.S.S. as co-inventors.

Received: December 8, 2023
Revised: April 8, 2024
Accepted: May 14, 2024
Published: May 15, 2024

REFERENCES

1. Rohaan, M.W., Wilgenhof, S., and Haanen, J.B.A.G. (2019). Adoptive cellular therapies: the current landscape. Virchows Arch. *474*, 449–461. https://doi.org/10.1007/s00428-018-2484-0.
2. Sterner, R.C., and Sterner, R.M. (2021). CAR-T cell therapy: current limitations and potential strategies. Blood Cancer J. *11*, 69. https://doi.org/10.1038/s41408-021-00459-7.
3. Morotti, M., Albukhari, A., Alsaadi, A., Artibani, M., Brenton, J.D., Curbishley, S.M., Dong, T., Dustin, M.L., Hu, Z., McGranahan, N., et al. (2021). Promises and challenges of adoptive T-cell therapies for solid tumours. Br. J. Cancer *124*, 1759–1776. https://doi.org/10.1038/s41416-021-01353-6.
4. Poorebrahim, M., Melief, J., Pico de Coaña, Y., L Wickström, S., Cid-Arregui, A., and Kiessling, R. (2021). Counteracting CAR T cell dysfunction. Oncogene *40*, 421–435. https://doi.org/10.1038/s41388-020-01501-x.
5. Vormittag, P., Gunn, R., Ghorashian, S., and Veraitch, F.S. (2018). A guide to manufacturing CAR T cell therapies. Curr. Opin. Biotechnol. *53*, 164–181. https://doi.org/10.1016/j.copbio.2018.01.025.
6. van Schalkwyk, M.C.I., van der Stegen, S.J.C., Bosshard-Carter, L., Graves, H., Papa, S., Parente-Pereira, A.C., Farzaneh, F., Fisher, C.D., Hope, A., Adami, A., and Maher, J. (2021). Development and Validation of a Good Manufacturing Process for IL-4-Driven Expansion of Chimeric Cytokine Receptor-Expressing CAR T-Cells. Cells *10*, 1797. https://doi.org/10.3390/cells10071797.
7. Rossy, J., Laufer, J.M., and Legler, D.F. (2018). Role of Mechanotransduction and Tension in T Cell Function. Front. Immunol. *9*, 2638. https://doi.org/10.3389/fimmu.2018.02638.
8. Hagihara, M., Higuchi, A., Tamura, N., Ueda, Y., Hirabayashi, K., Ikeda, Y., Kato, S., Sakamoto, S., Hotta, T., Handa, S., and Goto, S. (2004). Platelets, after Exposure to a High Shear Stress, Induce IL-10-Producing, Mature Dendritic Cells In Vitro. J. Immunol. *172*, 5297–5303. https://doi.org/10.4049/jimmunol.172.9.5297.
9. Mitchell, M.J., Lin, K.S., and King, M.R. (2014). Fluid Shear Stress Increases Neutrophil Activation via Platelet-Activating Factor. Biophys. J. *106*, 2243–2253. https://doi.org/10.1016/j.bpj.2014.04.001.
10. Li, R., Feng, D., Han, S., Zhai, X., Yu, X., Fu, Y., and Jin, F. (2023). Macrophages and fibroblasts in foreign body reactions: How mechanical cues drive cell functions? Mater. Today Bio *22*, 100783. https://doi.org/10.1016/j.mtbio.2023.100783.
11. Dombroski, J.A., Hope, J.M., Sarna, N.S., and King, M.R. (2021). Channeling the Force:

Piezo1 Mechanotransduction in Cancer Metastasis. Cells *10*, 2815. https://doi.org/10.3390/cells10112815.

12. Hwang, J.-R., Byeon, Y., Kim, D., and Park, S.-G. (2020). Recent insights of T cell receptor-mediated signaling pathways for T cell activation and development. Exp. Mol. Med. *52*, 750–761. https://doi.org/10.1038/s12276-020-0435-8.
13. Trebak, M., and Kinet, J.-P. (2019). Calcium signalling in T cells. Nat. Rev. Immunol. *19*, 154–169. https://doi.org/10.1038/s41577-018-0110-7.
14. Hope, J.M., Dombroski, J.A., Pereles, R.S., Lopez-Cavestany, M., Greenlee, J.D., Schwager, S.C., Reinhart-King, C.A., and King, M.R. (2022). Fluid shear stress enhances T cell activation through Piezo1. BMC Biol. *20*, 61. https://doi.org/10.1186/s12915-022-01266-7.
15. Goldsmith, M.A., and Weiss, A. (1988). Early Signal Transduction by the Antigen Receptor Without Commitment to T Cell Activation. Science *240*, 1029–1031. https://doi.org/10.1126/science.3259335.
16. Karttunen, J., and Shastri, N. (1991). Measurement of ligand-induced activation in single viable T cells using the lacZ reporter gene. Proc. Natl. Acad. Sci. USA *88*, 3972–3976. https://doi.org/10.1073/pnas.88.9.3972.
17. Wacholtz, M.C., and Lipsky, P.E. (1993). Anti-CD3-stimulated Ca2+ signal in individual human peripheral T cells. Activation correlates with a sustained increase in intracellular Ca2+1. J. Immunol. *150*, 5338–5349. https://doi.org/10.4049/jimmunol.150.12.5338.
18. Valitutti, S., Dessing, M., Aktories, K., Gallati, H., and Lanzavecchia, A. (1995). Sustained signaling leading to T cell activation results from prolonged T cell receptor occupancy. Role of T cell actin cytoskeleton. J. Exp. Med. *181*, 577–584. https://doi.org/10.1084/jem.181.2.577.
19. Timmerman, L.A., Clipstone, N.A., Ho, S.N., Northrop, J.P., and Crabtree, G.R. (1996). Rapid shuttling of NF-AT in discrimination of Ca2+ signals and immunosuppression. Nature *383*, 837–840. https://doi.org/10.1038/383837a0.
20. Wülfing, C., Rabinowitz, J.D., Beeson, C., Sjaastad, M.D., McConnell, H.M., and Davis, M.M. (1997). Kinetics and Extent of T Cell Activation as Measured with the Calcium Signal. J. Exp. Med. *185*, 1815–1825. https://doi.org/10.1084/jem.185.10.1815.
21. Hu, N.-W., Rodriguez, C.D., Rey, J.A., Rozenblum, M.J., Courtney, C.P., Balogh, P., Sarntinoranont, M., and Murfee, W.L. (2022). Estimation of shear stress values along endothelial tip cells past the lumen of capillary sprouts. Microvasc. Res. *142*, 104360. https://doi.org/10.1016/j.mvr.2022.104360.
22. Strony, J., Beaudoin, A., Brands, D., and Adelman, B. (1993). Analysis of shear stress and hemodynamic factors in a model of coronary artery stenosis and thrombosis. Am. J. Physiol. *265*, H1787–H1796. https://doi.org/10.1152/ajpheart.1993.265.5.h1787.
23. Quintana, A., Griesemer, D., Schwarz, E.C., and Hoth, M. (2005). Calcium-dependent activation of T-lymphocytes. Pflugers Arch. *450*, 1–12. https://doi.org/10.1007/s00424-004-1364-4.
24. Yang, P.-C., and Jafri, M.S. (2020). Ca2+ signaling in T lymphocytes: the interplay of the endoplasmic reticulum, mitochondria, membrane potential, and CRAC channels on transcription factor activation. Heliyon *6*, e03526. https://doi.org/10.1016/j.heliyon.2020.e03526.
25. Gnanasambandam, R., Ghatak, C., Yasmann, A., Nishizawa, K., Sachs, F., Ladokhin, A.S., Sukharev, S.I., and Suchyna, T.M. (2017). GsMTx4: Mechanism of Inhibiting Mechanosensitive Ion Channels. Biophys. J. *112*, 31–45. https://doi.org/10.1016/j.bpj.2016.11.013.
26. Mavligit, G.M., Hersh, E.M., and McBride, C.M. (1974). Lymphocyte blastogenesis induced by autochthonous human solid tumor cells: Relationship to stage of disease and serum factors. Cancer *34*, 1712–1721.
27. Grumont, R., Lock, P., Mollinari, M., Shannon, F.M., Moore, A., and Gerondakis, S. (2004). The Mitogen-Induced Increase in T Cell Size Involves PKC and NFAT Activation of Rel/NF-κB-Dependent c-myc Expression. Immunity *21*, 19–30. https://doi.org/10.1016/j.immuni.2004.06.004.
28. Böhmer, R.M., Bandala-Sanchez, E., and Harrison, L.C. (2011). Forward light scatter is a simple measure of T-cell activation and proliferation but is not universally suited for doublet discrimination. Cytometry *79A*, 646–652. https://doi.org/10.1002/cyto.a.21096.
29. Burkett, M.W., Shafer-Weaver, K.A., Strobl, S., Baseler, M., and Malyguine, A. (2005). A Novel Flow Cytometric Assay for Evaluating Cell-Mediated Cytotoxicity. J. Immunother. *28*, 396–402. https://doi.org/10.1097/01.cji.0000165357.11548.6d.
30. Vallabhapurapu, S., and Karin, M. (2009). Regulation and Function of NF-κB Transcription Factors in the Immune System. Immunology *27*, 693–733. https://doi.org/10.1146/annurev.immunol.021908.132641.
31. Schmitz, M.L., and Krappmann, D. (2006). Controlling NF-κB activation in T cells by costimulatory receptors. Cell Death Differ. *13*, 834–842. https://doi.org/10.1038/sj.cdd.4401845.
32. Mu, W., Wang, X., Zhang, X., Zhu, S., Sun, D., Ka, W., Sung, L.A., and Yao, W. (2015). Fluid Shear Stress Upregulates E-Tmod41 via miR-23b-3p and Contributes to F-Actin Cytoskeleton Remodeling during Erythropoiesis. PLoS One *10*, e0136607. https://doi.org/10.1371/journal.pone.0136607.
33. Makino, A., Shin, H.Y., Komai, Y., Fukuda, S., Coughlin, M., Sugihara-Seki, M., and Schmid-Schönbein, G.W. (2007). Mechanotransduction in leukocyte activation: a review. Biorheology *44*, 221–249.
34. Piechocka, I.K., Keary, S., Sosa-Costa, A., Lau, L., Mohan, N., Stanisavljevic, J., Borgman, K.J.E., Lakadamyali, M., Manzo, C., and Garcia-Parajo, M.F. (2021). Shear forces induce ICAM-1 nanoclustering on endothelial cells that impact on T-cell migration. Biophys. J. *120*, 2644–2656. https://doi.org/10.1016/j.bpj.2021.05.016.
35. Thomas, A., Daniel Ou-Yang, H., Lowe-Krentz, L., Muzykantov, V.R., and Liu, Y. (2016). Biomimetic channel modeling local vascular dynamics of pro-inflammatory endothelial changes. Biomicrofluidics *10*, 014101. https://doi.org/10.1063/1.4936672.
36. Tomida, T., Hirose, K., Takizawa, A., Shibasaki, F., and Iino, M. (2003). NFAT functions as a working memory of Ca2+ signals in decoding Ca2+ oscillation. EMBO J. *22*, 3825–3832. https://doi.org/10.1093/emboj/cdg381.
37. Gallagher, M.P., Conley, J.M., Vangala, P., Garber, M., Reboldi, A., and Berg, L.J. (2021). Hierarchy of signaling thresholds downstream of the T cell receptor and the Tec kinase ITK. Proc. Natl. Acad. Sci. USA *118*, e2025825118. https://doi.org/10.1073/pnas.2025825118.
38. Betts, M.R., and Koup, R.A. (2004). Detection of T-Cell Degranulation: CD107a and b. Methods Cell Biol. *75*, 497–512. https://doi.org/10.1016/s0091-679x(04)75020-7.
39. Feske, S., Giltnane, J., Dolmetsch, R., Staudt, L.M., and Rao, A. (2001). Gene regulation mediated by calcium signals in T lymphocytes. Nat. Immunol. *2*, 316–324. https://doi.org/10.1038/86318.
40. Cahalan, M.D., and Chandy, K.G. (2009). The functional network of ion channels in T lymphocytes. Immunol. Rev. *231*, 59–87. https://doi.org/10.1111/j.1600-065x.2009.00816.x.
41. Vaeth, M., Kahlfuss, S., and Feske, S. (2020). CRAC Channels and Calcium Signaling in T Cell-Mediated Immunity. Trends Immunol. *41*, 878–901. https://doi.org/10.1016/j.it.2020.06.012.
42. Jutz, S., Leitner, J., Schmetterer, K., Doel-Perez, I., Majdic, O., Grabmeier-Pfistershammer, K., Paster, W., Huppa, J.B., and Steinberger, P. (2016). Assessment of costimulation and coinhibition in a triple parameter T cell reporter line: Simultaneous measurement of NF-κB, NFAT and AP-1. J. Immunol. Methods *430*, 10–20. https://doi.org/10.1016/j.jim.2016.01.007.
43. Foletta, V.C., Segal, D.H., and Cohen, D.R. (1998). Transcriptional regulation in the immune system: all roads lead to AP-1. J. Leukoc. Biol. *63*, 139–152. https://doi.org/10.1002/jlb.63.2.139.
44. Crabtree, G.R. (2001). Calcium, Calcineurin, and the Control of Transcription. J. Biol. Chem. *276*, 2313–2316. https://doi.org/10.1074/jbc.r000024200.
45. Jain, J., McCaffrey, P.G., Valge-Archer, V.E., and Rao, A. (1992). Nuclear factor of activated T cells contains Fos and Jun. Nature *356*, 801–804. https://doi.org/10.1038/356801a0.
46. Liu, X., Berry, C.T., Ruthel, G., Madara, J.J., MacGillivray, K., Gray, C.M., Madge, L.A., McCorkell, K.A., Beiting, D.P., Hershberg, U., et al. (2016). T Cell Receptor-induced Nuclear Factor κB (NF-κB) Signaling and Transcriptional Activation Are Regulated by STIM1- and Orai1-mediated Calcium Entry. J. Biol. Chem. *291*, 8440–8452. https://doi.org/10.1074/jbc.m115.713008.
47. Ramesh, P., Shivde, R., Jaishankar, D., Saleiro, D., and Le Poole, I.C. (2021). A Palette of Cytokines to Measure Anti-Tumor Efficacy of T Cell-Based Therapeutics. Cancers *13*, 821. https://doi.org/10.3390/cancers13040821.
48. Hoekstra, M.E., Vijver, S.V., and Schumacher, T.N. (2021). Modulation of the tumor micro-environment by CD8+ T cell-derived cytokines. Curr. Opin. Immunol. *69*, 65–71. https://doi.org/10.1016/j.coi.2021.03.016.
49. Liu, C.S.C., Raychaudhuri, D., Paul, B., Chakrabarty, Y., Ghosh, A.R., Rahaman, O.,

Talukdar, A., and Ganguly, D. (2018). Cutting Edge: Piezo1 Mechanosensors Optimize Human T Cell Activation. J. Immunol. *200*, 1255–1260. https://doi.org/10.4049/jimmunol.1701118.

50. Jairaman, A., Othy, S., Dynes, J.L., Yeromin, A.V., Zavala, A., Greenberg, M.L., Nourse, J.L., Holt, J.R., Cahalan, S.M., Marangoni, F., et al. (2021). Piezo1 channels restrain regulatory T cells but are dispensable for effector CD4+ T cell responses. Sci. Adv. *7*, eabg5859. https://doi.org/10.1126/sciadv.abg5859.
51. Alessandri-Haber, N., Dina, O.A., Chen, X., and Levine, J.D. (2009). TRPC1 and TRPC6 Channels Cooperate with TRPV4 to Mediate Mechanical Hyperalgesia and Nociceptor Sensitization. J. Neurosci. *29*, 6217–6228. https://doi.org/10.1523/jneurosci.0893-09.2009.
52. Bae, C., Sachs, F., and Gottlieb, P.A. (2011). The Mechanosensitive Ion Channel Piezo1 Is Inhibited by the Peptide GsMTx4. Biochemistry *50*, 6295–6300. https://doi.org/10.1021/bi200770q.
53. Nikolaev, Y.A., Cox, C.D., Ridone, P., Rohde, P.R., Cordero-Morales, J.F., Vásquez, V., Laver, D.R., and Martinac, B. (2019). Mammalian TRP ion channels are insensitive to membrane stretch. J. Cell Sci. *132*, jcs238360. https://doi.org/10.1242/jcs.238360.
54. Mitchell, M.J., and King, M.R. (2013). Fluid shear stress sensitizes cancer cells to receptor-mediated apoptosis via trimeric death receptors. New J. Phys. *15*, 015008. https://doi.org/10.1088/1367-2630/15/1/015008.

STAR★METHODS

KEY RESOURCES TABLE

REAGENT or RESOURCE	SOURCE	IDENTIFIER
Antibodies		
For confocal microscopy: Phospho-Nf-κB P65 (Ser536) Monoclonal Antibody (Host: Rabbit, clone: T.849.2)	Thermo Fisher Scientific	Cat#:MA5-15160; RRID:AB_10983078
For confocal microscopy: Phospho-c-Fos (Ser32) Recombinant Monoclonal Antibody (Host: Rabbit, clone: cFosS32-BA9)	Thermo Fisher Scientific	Cat#:MA5-37421; RRID:AB_2897355
For confocal microscopy: NFATc1 Polyclonal Antibody (Host: Rabbit)	Novus Biologicals	Cat#:NB100-56732; RRID:AB_838619
For confocal microscopy: Ki-67 Recombinant Monoclonal Antibody (Host: Rabbit, clone: SP6)	Abcam	Cat#:ab16667; RRID:AB_302459
For confocal microscopy: Goat Anti-Rabbit IgG (H+L) Polyclonal Secondary Antibody - Alexa Fluor 488	Molecular Probes	Cat#:A-11008; RRID:AB_143165
For flow cytometry: CD4 Monoclonal Antibody (Host: Mouse, clone: RPA-T4) - APC	Thermo Fisher Scientific	Cat#:17-0049-42; RRID:AB_1272048
For flow cytometry: CD8a Monoclonal Antibody (Host: Mouse, clone: RPA-T8) - FITC	Thermo Fisher Scientific	Cat#:11-0088-42; RRID:AB_10669559
For flow cytometry: Human TruStain FcX	BioLegend	Cat#:422301; RRID:AB_2818986
For flow cytometry: Phospho-NFkB p65 (Ser529) Monoclonal Antibody (Host: Mouse; clone: B33B4WP) - PE	Thermo Fisher Scientific	Cat#:12-9863-42; RRID:AB_2572751
For flow cytometry: CD69 Monoclonal Antibody (Host: Mouse; clone: FN50) - FITC	BD Biosciences	Cat#:555530; RRID:AB_395915
For flow cytometry: CD25 Monoclonal Antibody (Host: Mouse; clone: CD25-4E3) - APC	Thermo Fisher Scientific	Cat#:17-0257-42; RRID:AB_11218671
For flow cytometry: CD107a (LAMP-1) Monoclonal Antibody (Host: Mouse; clone: eBioH4A3) - Alexa Fluor™ 488	Thermo Fisher Scientific	Cat#53-1079-42; RRID:AB_2016657
For flow cytometry: IFN gamma Monoclonal Antibody (Host: Mouse; clone: 4S.B3) - PE	Thermo Fisher Scientific	Cat#:12-7319-41; RRID:AB_1311250
For flow cytometry: TNF alpha Monoclonal Antibody (Host: Mouse; clone: MAb11) - PE	Thermo Fisher Scientific	Cat#:12-7349-41; RRID:AB_10668834
For flow cytometry: IL-2 Monoclonal Antibody (Host: Rat; clone: MQ1-17H12) - PE	Thermo Fisher Scientific	Cat#:12-7029-41; RRID:AB_10801952
For flow cytometry: Ki-67 Monoclonal Antibody (Host: Mouse; clone: Ki-67) - Alexa Fluor® 488	BioLegend	Cat#:350508; RRID:AB_10933085
For flow cytometry: Annexin V - FITC	BD Biosciences	Cat#:556419; RRID:AB_2665412
For flow cytometry: Propidium Iodide Staining Solution	BD Biosciences	Cat#:556463; RRID:AB_2869075
For flow cytometry: Cd8a Monoclonal Antibody (Host: Mouse; clone: RPA-T8) - APC	Thermo Fisher Scientific	Cat#:17-0088-42; RRID:AB_10669564
For flow cytometry: Granzyme B Monoclonal Antibody (Host: Mouse; clone: N4TL33) - PE	Thermo Fisher Scientific	Cat#:12-8896-42; RRID:AB_2724394
For flow cytometry: Perforin Monoclonal Antibody (Host: Mouse; clone: dG9) - eFluor 450,	Thermo Fisher Scientific	Cat#:48-9994-42; RRID:AB_2574145
Chemicals, peptides, and recombinant proteins		
RPMI 1640 media 1x with L-glutamine	Corning	Cat#:10-040-CV

(*Continued on next page*)

Continued

REAGENT or RESOURCE	SOURCE	IDENTIFIER
Fetal bovine serum	Gibco	Cat#:16140071
Pen/Strep	Gibco	Cat#:15140-122
HEPES	Sigma Aldrich	Cat#:H4034-100G
Hanks' Balanced Salt Solution (HBSS) w/o Calcium/Magnesium	Gibco	Cat#:14175095
Hanks' Balanced Salt Solution (HBSS), with Calcium/Magnesium	Gibco	Cat#:14025092
Ficoll® Paque	Cytiva	Cat#:17-1440-02
Paraformaldehyde	Electron Microscopy Sciences	Cat#:15714S
Triton-X-100	Sigma Aldrich	Cat#:9002-93-1
Bovine serum albumin	Sigma Aldrich	Cat#:A1470-100G
Antifade mounting media	Vectrashield	Cat#:H-1000
Methanol	Fisher Chemical	Cat#:A465-4
TWEEN® 20	Sigma Aldrich	Cat#:P1379
GolgiPlug™ Protein Transport Inhibitor	Fisher Scientific	Cat#:BDB555029
Pluronic™ F-127	Thermo Fisher Scientific	Cat#:P3000MP
GsMTx-4	Abcam	Cat#:ab141871
Dapi	Sigma Aldrich	Cat#:D9542-5MG
Normal Goat Serum (10%)	Thermo Fisher Scientific	Cat#:50-062Z
eBioscience Intracellular Fixation & Permeabilization Buffer Set	Thermo Fisher Scientific	Cat#:88-8824-00
Critical commercial assays		
Human Pan T Cell isolation kit	Miltenyi Biotech	Cat#:130-096-535
Human $CD8^+$ T Cell isolation kit	Miltenyi Biotech	Cat#:130-096-495
Dynabeads™ Human T-Activator CD3/CD28	Gibco	Cat#:11-161-D
Fluo-4, AM, cell permeant	Thermo Fisher Scientific	Cat#:F14201
Violet Proliferation Dye 450	BD Horizon	Cat#:562158; RRID:AB_2869398
Actinred™ 555 Readyprobes™	Thermo Fisher Scientific	Cat#:R37112
IFN-gamma ELISA Kit	BioLegend	Cat#:430104
TNF-alpha ELISA Kit	BioLegend	Cat#:430204
IL-2 ELISA Kit	BioLegend	Cat#:431804
Software and algorithms		
Source data and statistical analysis	This paper	Tables S1, S2, S3, S4, S5, S6, and S7
Code for confocal microscopy analysis	This paper	https://github.com/nicolesarna/TCellAnalysis
Software and algorithms		
GraphPad Prism v10.1	GraphPad Software Inc.	RRID:SCR_002798
Fiji – ImageJ	FIJI	RRID:SCR_002285
FlowJo v10.8.2	FlowJo	RRID:SCR_008520
MATLAB_R2023a	MathWorks	RRID:SCR_001622
Bio-Formats	Open Microscopy Environment	RRID:SCR_000450
Microsoft PowerPoint v16.78	Microsoft	RRID:SCR_023631
Microsoft Excel v16.78	Microsoft	RRID:SCR_016137
Other		
MS Columns	Miltenyi Biotech	Cat#:130-042-201
OctoMACS™ Separator	Miltenyi Biotech	Cat#:130-042-109

(*Continued on next page*)

Continued

REAGENT or RESOURCE	SOURCE	IDENTIFIER
MACS® MultiStand	Miltenyi Biotech	Cat#:130-042-303
MACS® BSA Stock Solution	Miltenyi Biotech	Cat#:130-091-376
Shandon Cytospin 3 Centrifuge	Marshall Scientific	Cat#:TH-CYTO3; RRID:SCR_020507
18mm Round Glass Coverslips	Electron Microscopy Sciences	Cat#:71887-06
Glass slides	VWR	Cat#:48311-703
Citrate Collection Tube	BD	Cat#:363083
EDTA Collection Tube	BD	Cat#:366643
Cytology Funnels	Fisher Scientific	Cat#:10-354
Super Pap Pen	Electron Microscopy Sciences	Cat#:71312

RESOURCE AVAILABILITY

Lead contact

Further information on resources and reagents should be directed to the lead contact, Dr. Michael R. King (mike.king@rice.edu).

Materials availability

No unique materials were generated in this study. Further inquiries should be directed to the lead contact, Dr. Michael R. King (mike.king@rice.edu).

Data and code availability

- All data presented in this study will be shared upon reasonable request by the lead contact, Dr. Michael R. King (mike.king@rice.edu).
- All original code has been deposited at https://github.com/nicolesarna/TCellAnalysis and is publicly available as of the date of publication. DOIs are listed in the key resources table. The authors request that these programs not be modified or distributed without attribution to this published work.
- Any additional information required to reanalyze the data reported in this paper is available from the lead contact upon request.

EXPERIMENTAL MODEL AND STUDY PARTICIPANT DETAILS

Human subject details

Whole blood samples were collected from volunteers after informed consent under Vanderbilt University Institutional Review Board (IRB) approved protocol #170222. Consideration was given to obtain samples from both biological sexes in the young adult age range. Participants ranged from 19-34 (self-reported), include male and female (self-reported), and declared no health conditions (self-reported). Information regarding ancestry, race, and ethnicity was not collected in this study. Once samples were collected from the donor at the Vanderbilt University Medical Center phlebotomy lab, donor samples were deidentified. Biological sex is included with raw data provided in Tables S1, S2, S3, S4, S5, and S6. where applicable. Whole blood samples were obtained from each patient in EDTA collection tubes and processed within 24 hours. For experiments evaluating calcium influx, sodium citrate collection tubes were used.

METHOD DETAILS

Cell culture

Primary T cells were cultured in RPMI Medium 1640 with 2 mM L-Glutamine (Corning), 25mM HEPES (Sigma Aldrich), 10% FBS (Gibco), and 1% penicillin streptomycin (Gibco) in a water-jacketed incubator at 37°C and 5% CO_2. T cells were cultured in 24-well or 12-well polystyrene-treated culture plates and maintained at a density of 200,000-400,000 cells/mL.

T Cell isolation and activation

Primary T cells were isolated from peripheral blood mononuclear cells (PBMCs) through Ficoll® Paque density gradient centrifugation (Cytiva) and T cells were magnetically separated via negative selection using the Human Pan T Cell isolation kit (Miltenyi Biotech). T cells were activated with or without Dynabeads Human T-Activator CD3/CD28 magnetic beads (αCD3/CD28) (Gibco) according to the manufacturer's instructions, maintaining a bead-to-cell ratio of 1:1. T cells treated with Dynabeads were incubated at 37°C for 15 min before loading into cone-and-plate viscometers (Brookfield). Both Dynabead-treated and untreated T cells were subjected to 5 dyn/cm^2 FSS for 1 hr in the cone-and-plate viscometers. The static (non-FSS) T cell samples were also loaded into viscometers to replicate identical conditions and environment as sheared groups, with the viscometer turned off. Of note, bead-bound αCD3/CD28 were maintained in the T cell culture for the duration of experiments.

Fluid shear stress experiments were carried out following the methodology described previously.[54] Briefly, cone-and-plate viscometers were thoroughly cleaned with 70% ethanol immediately prior to use and both the cone and the plate were blocked with 5% BSA (Sigma Aldrich) for 1 hr to prevent non-specific binding. Then, BSA was removed and a 2mL suspension of T cells in complete RPMI was added at a concentration of 500,000-700,000 cells/mL. Where indicated, T cells treated with GsMTX-4 were resuspended in GsMTX-4 (Abcam) supplemented media (2.5μM) immediately before the addition of bead-bound αCD3/CD28 and FSS exposure. Immediately following the 1hr FSS activation, static and shear samples were resuspended in fresh media, plated, and cultured.

Flow cytometry sample preparation

All flow cytometry measurements were conducted in a Guava easyCyte 12HT flow cytometer (Millipore) and quantified using FlowJo software (RRID:SCR_008520) following the gating strategy shown in Figure S4. Samples were collected and centrifuged at 300g for 5 min. When staining for surface markers CD4 (Thermo Fisher Scientific, RPA-T4), CD8a (Thermo Fisher Scientific, RPA-T8), CD69 (BD Biosciences, FN50), and CD25 (Thermo Fisher Scientific, CD25-4E3), cell pellets were resuspended in 1% BSA and incubated with Human TruStain FcX Blocker (BioLegend) for 10 minutes at RT. Immediately after, cells were incubated with the fluorochrome conjugated antibody at RT for 15 min in the dark.

When staining for intracellular proteins, including phospho-NF-κB (Thermo Fisher Scientific, B33B4WP), CD107a (Thermo Fisher Scientific, eBioH4A3), and Ki-67 (BioLegend, Ki-67) cells were fixed for 10 min in 4% paraformaldehyde (PFA) (Electron Microscopy Sciences) at room temperature (RT). Samples were washed in HBSS (w/o Ca^{2+}/Mg^{2+}) (Gibco) then permeabilized in 100% methanol (Fisher Chemical) on ice for 10 min. Cells were washed again, resuspended in 1% BSA, and incubated with the fluorochrome-conjugated antibody for 15 min at RT in the dark. To quantify cytokine secretion, T cells were incubated with GolgiPlug™ Protein Transport Inhibitor (Fisher Scientific) for 4 hr prior to fixation and permeabilization. Antibodies for IFN-γ (4S.B3), TNF-α (MAb11), and IL-2 (MQ1-17H12), were obtained from Thermo Fisher Scientific.

After staining, samples were centrifuged, resuspended in 200μL HBSS (w/o Ca^{2+}/Mg^{2+}), and plated in a clear, U bottom 96-well plate.

Annexin V/PI assay

To evaluate cell death, an Annexin V (AV) and propidium iodide (PI) (BD Biosciences) assay was performed and quantified via flow cytometry. AV binds to extracellular proteins expressed during early stages of apoptosis and PI binds to DNA accessed through a damaged membrane which is indicative of necrosis and late-stage apoptosis. T cells were collected immediately after FSS exposure and washed with HBSS (w/o Ca^{2+}/Mg^{2+}). Cells were then resuspended in 100μL of the staining solution (2 AV: 5 PI: 93 HBSS w/ Ca^{2+}/Mg^{2+}) and incubated at RT for 15 min in the dark. Cells were then centrifuged at 300g for 5 min, resuspended in 200μL HBSS (w/ Ca^{2+}/Mg^{2+}), and prepared for flow cytometry.

Intracellular calcium assay

Fluo-4 AM cell permeant (Thermo Fisher Scientific) was used in flow cytometry to evaluate intracellular calcium levels. Fluo-4 dye was solubilized in Pluronic F-127 (Thermo Fisher Scientific) solution to a concentration of 1M. Cell samples were washed in HBSS (w/o Ca^{2+}/Mg^{2+}) then resuspended in HBSS (w/ Ca^{2+}/Mg^{2+}) and incubated with 1μM Fluo-4 for 30 min at 37°C. Immediately following staining, cells were centrifuged at 300g for 5 min, resuspended in HBSS (w/ Ca^{2+}/Mg^{2+}) and loaded into well plates for flow cytometry.

Cell proliferation assay

To evaluate T cell proliferation, a violet proliferation dye (VPD450) (BD) was introduced to the cells immediately following activation, according to the manufacturer's instructions. Briefly, cells were washed three times in HBSS (w/o Ca^{2+}/Mg^{2+}) and labeled with 1μM VPD450 for 15 min at 37°C. Cells were washed in HBSS (w/o Ca^{2+}/Mg^{2+}) three additional times and loaded into well plates for 72 hr in appropriate cell culture conditions.

Nonfluorescent VPD450 passively diffuses through the cell membrane and becomes fluorescent when it binds to protein amide groups in viable cells. As cells divide, VPD450 is uniformly distributed to each daughter cell, retaining approximately half of the fluorescent dye from its parent cell. In this manner, the daughter cell generation can be identified as discrete, lower intensity peaks in flow cytometry (excitation: 405nm, emission: 450nm).

ELISA assay

At 3 days post-activation, T cell media was harvested and T cells were counted at the time of collection. IFN-γ, TNF-α, and IL-2 ELISAs were performed in accordance with the manufacturer's guidelines, where the coating antibody was allowed to incubate overnight at 37°C, and the ELISA was performed the following day. For the IFN-γ ELISA, dilutions were performed by adding 100 μL of T cell media to 900 mLs of Assay Diluent A. The TNF-α ELISA required samples to be diluted by adding 200 μL of media to 800 mL of Assay Diluent A. The IL-2 ELISA required 2 dilutions to be performed by adding 25 μL and 10 μL of media to 975 mL and 990 mL of Assay Diluent A, respectively. The different dilution used was accounted for during analysis (see Table S5). All standard and sample wells were run in triplicate. The absorbance of the ELISA plate was read at 450 nm and 570 nm following the addition of the stop solution by a plate reader. Analysis and standard curves were generated to quantify the total cytokine levels (pg) present in the media and normalized to cell number at the time of media collection.

Confocal microscopy slide preparation

At the indicated timepoints, T cells were collected from culture and washed in HBSS (w/o Ca^{2+}/Mg^{2+}) three times. Samples were then fixed in 4% PFA for 15 min at RT and resuspended in 1% BSA. The Thermo Shandon Cytospin 3 was used at 1000RPM for 4 min to spin T cells onto glass slides (VWR) and a hydrophobic pen (Electron Microscopy Sciences) was used to draw a circle around the sample to confine it. Slides were set to dry at RT for at least one hour. Unless otherwise indicated, the washing step for all microscopy slides consisted of three washes in a 0.02% Tween20 (Sigma Aldrich) in HBSS (w/o Ca^{2+}/Mg^{2+}) solution for 5 min per wash. Cells were permeabilized in 1X Triton (Sigma Aldrich) for 10 min. Samples were washed, blocked using 5% BSA and 5% goat serum (Thermo Fisher Scientific) for 1 hr at RT, then incubated at 4°C overnight with the indicated primary antibody. Following the overnight incubation, cells were washed three times and incubated at RT in the dark with the indicated secondary antibody, DAPI (1:1000) (Sigma Aldrich), and ActinRed™ 555 ReadyProbes™ reagent (Thermo Fisher Scientific) for 45 min at RT. The primary antibodies used for confocal microscopy include phospho-Nf-κB (Thermo Fisher Scientific, T.849.2), phospho-c-Fos (Thermo Fisher Scientific, cFosS32-BA9), NFATc1 (Novus Biologicals), and Ki-67 (Abcam, SP6). The Goat Anti-Rabbit IgG (H+L) Secondary Antibody (Molecular Probes) was used for all confocal microscopy slides. Cells were washed three additional times and 1mm coverslips (Electron Microscopy Sciences) were mounted using anti-fade mounting medium (Vectrasheild) and sealed with nail polish. Slides were imaged using a Zeiss LSM900 confocal microscope with a 63X oil immersion objective.

Confocal image presentation

All representative confocal images were rendered in Fiji, where brightness and contrast were modified across the entire image (in a linear fashion) for ease of viewing. Scale bars were cut from the original images and then pasted in a more visible position on the final composite images via Microsoft Powerpoint (Microsoft).

MATLAB image analysis algorithm

We developed two MATLAB algorithms for the quantitative analysis of fluorescence intensity in confocal microscopy images. The first algorithm ('CellAnalysis.m') was designed to assess fluorescence within the entire cell body and was employed for quantifying phospho- NF-κB and c-Fos. The workflow for this algorithm is illustrated in Figure S5A. Additionally, we adapted the program to quantify fluorescence within the nucleus ('NucleusAnalysis.m'), used for the analysis of NFAT and Ki67, to determine protein translocation into the nucleus. The corresponding workflow is depicted in Figure S5B.

Confocal images were loaded into MATLAB (MathWorks) using Bio-Formats (Open Microscope Environment), to read and process Zeiss .czi microscopy files. The program is equipped with a graphical user interface (GUI) that allows the user to select multiple images for batch processing. Image pre-processing was performed on individual image planes to create masks to overlay onto the original image planes for fluorescence analysis. Image pre-processing employed thresholding and noise-removal functions to refine cell regions, where these parameters were applied consistently across all images.

The nuclear stain (DAPI) plane served to segment individual cells, creating distinct regions of interest (ROIs) by drawing ridge lines using the watershed function. For whole-cell analysis, these watershed ridge lines were imposed on the cell body (F-actin) mask. Subsequently, the segmented mask was overlaid onto the original, untouched plane containing the protein of interest. Each cell or nucleus ROI was evaluated using the regionprops function. Fluorescence intensity was calculated by first quantifying the integrated density (IntDensity) of each ROI using Equation 1:

$$IntDensity_{ROI} = Area_{ROI} \times Mean_{ROI} \quad \text{(Equation 1)}$$

All fluorescence data are presented in terms of the CTCF, calculated by Equation 2:

$$CTCF = IntDensity_{ROI} - Area_{ROI} \times Mean_{Bkg} \quad \text{(Equation 2)}$$

QUANTIFICATION AND STATISTICAL ANALYSIS

All data are presented as mean ± standard error of the mean (SEM), unless otherwise indicated. A difference was considered statistically significant with a p-value less than 0.05. Unless otherwise stated, the analysis of variance (ANOVA) statistical test was performed to compare more than two groups using Tukey's multiple comparison test. For bar graphs comparing T cell activation conditions (Static, FSS, Static+αCD3/CD28, FSS+anti-CD3/CD28), each point within a condition represents an independent experiment using T cells obtained from a unique donor. For confocal imaging fluorescence analysis, statistical outliers were identified and removed before final analysis using the robust regression and outlier removal (ROUT) method with Q (maximum desired false discovery rate) = 1%. All graph creation and statistical analyses were performed in GraphPad Prism (Version 10.1.0, GraphPad Software Inc.) with figure source data and analyses in supplemental information.